Journal of Hazardous Materials 424 (2022) 127447

Contents lists available at ScienceDirect

Journal of Hazardous Materials

journal homepage: www.elsevier.com/locate/jhazmat

# Treatment of cylindrospermopsin by hydroxyl and sulfate radicals: Does degradation equal detoxification?

Marcel Schneider [a,b,*], Marina F. Grossi [a], Darshak Gadara [a], Zdeněk Spáčil [a], Pavel Babica [a], Luděk Bláha [a]

[a] RECETOX, Faculty of Science, Masaryk University, Kotlarska 2, 61137 Brno, Czech Republic
[b] Leibniz Institute for Plasma Science and Technology (INP), Felix-Hausdorff-Straße 2, 17489 Greifswald, Germany

## HIGHLIGHTS

- $SO_4^{-}$• was more effective for the degradation of cylindrospermopsin than •OH.
- Degradation mechanisms of both radical species were similar.
- Cylindrospermopsin treatment by both radicals led to almost complete detoxification.
- Some degradation products may still be toxic to the in vitro liver model.
- *In vitro* 3D models can sensitively assess toxicity in water treatment applications.

## GRAPHICAL ABSTRACT

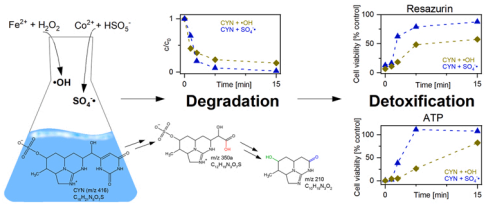


## ARTICLE INFO

Editor: Sungjun Bae

*Keywords:*
advanced oxidation process
cyanotoxin
hepatospheroid
toxicity
water treatment

## ABSTRACT

Drinking water treatment ultimately aims to provide safe and harmless drinking water. Therefore, the suitability of a treatment process should not only be assessed based on reducing the concentration os a pollutant concentration but, more importantly, on reducing its toxicity. Hence, the main objective of this study was to answer whether the degradation of a highly toxic compound of global concern for drinking water equals its detoxification. We, therefore, investigated the treatment of cylindrospermopsin (CYN) by •OH and $SO_4^{-}$• produced in Fenton and Fenton-like reactions. Although $SO_4^{-}$• radicals removed the toxin more effectively, both radical species substantially degraded CYN. The underlying degradation mechanisms were similar for both radical species and involved hydroxylation, dehydrogenation, decarboxylation, sulfate group removal, ring cleavage, and further fragmentation. The hydroxymethyl uracil and tricyclic guanidine moieties were the primary targets. Furthermore, the residual toxicity, assessed by a 3-dimensional human in vitro liver model, was substantially reduced during the treatment by both radical species. Although the results indicated that some of the formed degradation products might still be toxic, the overall reduction of the toxicity together with the proposed degradation pathways allowed us to conclude: "*Yes, degradation of CYN equals its detoxification!*".

* Corresponding author at: Leibniz Institute for Plasma Science and Technology (INP), Felix-Hausdorff-Straße 2, 17489 Greifswald, Germany.
*E-mail addresses:* marcel.schneider@inp-greifswald.de, marcel.schneider90@outlook.com (M. Schneider), marina.grossi@recetox.muni.cz (M.F. Grossi), darshak.gadara@recetox.muni.cz (D. Gadara), zdenek.spacil@recetox.muni.cz (Z. Spáčil), pavel.babica@recetox.muni.cz (P. Babica), ludek.blaha@recetox.muni.cz (L. Bláha).

https://doi.org/10.1016/j.jhazmat.2021.127447
Received 16 July 2021; Received in revised form 4 October 2021; Accepted 5 October 2021
Available online 16 October 2021

## 1. Introduction

Cyanobacteria are bloom-forming phototrophic prokaryotes that can produce various secondary metabolites, including taste and odor, and toxic compounds. In recent years, due to increased eutrophication of surface water, toxic cyanobacterial blooms occurred more frequently, including massive harmful algal blooms and global toxicity outbreaks (Brooks et al., 2016). This consequently increased the risk for cyanotoxin-contaminated drinking water. Besides the well-studied microcystin-LR, other cyanotoxins like the hepatotoxin cylindrospermopsin (CYN), which was initially assumed to be primarily found in tropical regions, are now also detected in non-tropical areas like Central Europe (Blahova et al., 2021). Moreover, Scarlett et al. (2020) reported that CYN concentrations detected in surface water regularly exceeded a value of 0.5 μg $L^{-1}$ in Asia and the Pacific region (68.5%), Europe (49.9%), North America (40.8%), and South America (68.5%). Recognizing CYN as a potential threat to human and animal health, the World Health Organization just recently proposed guideline values of 0.7 μg $L^{-1}$ and 3.0 μg $L^{-1}$ for chronic and short-term exposure, respectively, for CYN for drinking water (World Health Organization, 2020). Furthermore, as CYN can persist in surface water for up to several weeks (Ministry of Health, 2017), appropriate treatment methods are inevitable to remove the hepatotoxin and provide safe and toxin-free drinking water.

Advanced oxidation processes (AOPs) are amongst the approaches for removing CYN from drinking water that yield promising results. Different AOPs have been studied, including UV/$H_2O_2$ (He et al., 2014b), UV/$S_2O_8^{2-}$ and UV/$HSO_5^-$ (He et al., 2014a), photocatalysis (Fotiou et al., 2015; Zhang et al., 2015b), $TiO_2$-catalyzed ozonation (Wu et al., 2015), Fenton-like oxidation (Liu et al., 2018), and non-thermal plasmas (Schneider et al., 2020). Although all studied AOPs were relatively effective for removing CYN under experimental conditions, they all come with certain practical, environmental, and economic advantages and disadvantages (Schneider and Bláha, 2020). Fenton (-like) oxidation is a handy tool for laboratory-scale studies, e.g., for investigating underlying degradation mechanisms, because the experimental conditions can be easily controlled and the mechanisms of radical production have been extensively studied (Anipsitakis and Dionysiou, 2004; Bokare and Choi, 2014; Ike et al., 2018; Ji et al., 2019; Zeng et al., 2020).

The most commonly studied variant of the Fenton reaction uses the so-called Fenton's reagent, i.e., $Fe^{2+}$ and $H_2O_2$, to produce hydroxyl radicals (•OH). However, when employing sulfate-containing peroxides like peroxymono- or -disulfate (PMS and PS) instead, sulfate radicals ($SO_4^-$•) can be formed in a Fenton-like reaction. Anipsitakis and Dionysiou (2004) examined the activation of PMS and PS by different transition metals and identified $Co^{2+}$ and $Ag^+$, respectively, to be the most effective catalysts. The $SO_4^-$• was shown to be more selective than the •OH, which, similar to ozone, may make it more suitable for water treatment in the presence of high natural organic matter content (Schneider and Bláha, 2020). Additionally, due to its higher selectivity, the $SO_4^-$• has a longer half-life of about 30–40 μs compared to the •OH (0.02 μs) (Ghanbari and Moradi, 2017). Furthermore, it has a higher redox potential across a broader pH range and the precursor peroxides PMS and PS are more stable than $H_2O_2$, which increases their transportability and storability (Schneider and Bláha, 2020). Under certain conditions, e.g., under alkaline pH or in the presence of water, PMS can simultaneously produce $SO_4^-$• and •OH as primary and secondary species (Schneider and Bláha, 2020). Despite these advantages over •OH, $SO_4^-$•-based AOPs are still less commonly studied and used for water treatment (Ike et al., 2018).

The effective degradation of CYN by different oxidants, including •OH and $SO_4^-$•, has been reported before, and some degradation mechanisms and pathways for the reaction of CYN with both radical species have been proposed based on tentatively identified degradation products (He et al., 2014b). However, to the best of our knowledge, a direct comparison of •OH and $SO_4^-$•-based degradation of CYN and underlying mechanisms under similar reaction conditions has not been studied.

Furthermore, the treatment of water containing pollutants and toxins leads to various potentially toxic transformation products (Neale et al., 2020). However, the residual toxicity of treated CYN and formed degradation products has only rarely been examined, and, therefore, we posed the question: "*Does degradation equal detoxification?*".

Concerning the toxicity of CYN, findings from Banker et al. (2001) showed that the uracil moiety of CYN is often associated with its toxicity. The alteration of the uracil group by as much as the substitution of one hydrogen atom by one chlorine atom decreased the toxicity of the degradation product ($LD_{50}$ > 10,000 μg/kg) by a factor of 50 compared with the parent toxin ($LD_{50}$ = 200 μg/kg) after intraperitoneal injection in mice (Banker et al., 2001). However, they identified only two degradation products and purified them before administration to the mice. In addition to the uracil moiety, the guanidine structure and the hydroxyl group, which is bond to the methylene group that connects the uracil moiety with the tricyclic system, have recently also been shown to be involved in the toxicity of CYN (Cartmell et al., 2017; Evans et al., 2019). Although more than 100 potential CYN degradation products have been reported so far, also due to more advanced analytical instrumentation, information on the toxicity of the treated compound mixture is still scarce.

A limited number of recent studies assessed the residual toxicity after treatment of CYN, for example, using genetically engineered yeast cells to evaluate estrogenicity (Liu et al., 2018) or human intestinal cells (Merel et al., 2010). However, as CYN primarily targets the liver and kidney and is thus often categorized as a hepatotoxin, CYN toxicity is commonly examined in vivo in rodent liver or employing in vitro liver cell models (Scarlett et al., 2020). *In vivo* hepatotoxicity to mice was examined after intragluteal injection of photocatalytically treated CYN (Wang et al., 2019). However, human liver cell lines HepG2 or HepG2/C3A were most often employed to study in vitro hepatotoxicity of CYN treated, e.g., by ozonation (Yan et al., 2016), photocatalysis (Wang et al., 2019; Zhang et al., 2015b), or biodegradation (Martínez-Ruiz et al., 2020).

However, in vitro cell systems in two-dimensional (2D) monolayer cultures used in these studies do not adequately recapitulate some of the critical characteristics of human hepatocytes. Cells in 2D monolayers appear to be less sensitive to the toxicity of CYN or its degradation products compared to primary rodent hepatocytes (López-Alonso et al., 2013), differentiated HepaRG cells (Martínez-Ruiz et al., 2020), or three-dimensional (3D) cultures of human liver stem cells (Basu et al., 2018). 3D cell cultures emulate the in vivo-like microenvironment and cell-cell and cell-extracellular matrix interactions better (Zhang et al., 2020). Moreover, they provide a higher physiological relevance and can predict organ- and tissue-specific in vivo responses more accurately (Basu et al., 2020; Zhang et al., 2020). Scaffold-free spheroids represent a 3D culture method well-suited for cost-effective toxicity assessment and drug screening (Basu et al., 2020; Costa et al., 2016), and recently, spheroid cultures of HepG2 or HepG2/C3A cells were successfully used to study hepatotoxic mechanisms of CYN (Hercog et al., 2020; Štampar et al., 2021).

In this study, we investigated CYN degradation by Fenton and Fenton-like oxidation using the following transition metal and oxidant combinations: i) $Fe^{2+}$/$H_2O_2$, ii) $Co^{2+}$/PMS, and iii) $Ag^+$/PS to answer whether degradation equals detoxification. This study aimed to investigate and compare the degradation mechanisms and pathways and assess the residual hepatotoxicity of the treated CYN and its degradation products. Therefore, after optimizing the most suitable treatment conditions concerning the CYN degradation effectivity, the degradation pathways were proposed based on tentatively identified degradation products. The contribution of •OH and $SO_4^-$• to the CYN degradation was examined using ethanol (EtOH) and tert-butanol (tBuOH) as radical quenchers to better understand the underlying degradation mechanisms. Lastly, the residual hepatotoxicity of the treated CYN solutions

was assessed using 3D HepG2 spheroids as a relevant human liver model. To the best of our knowledge, this is the first study to assess the residual toxicity of CYN treated by $SO_4^{-}$• radicals.

## 2. Materials and methods

### 2.1. Standards and reagents

Dry CYN (≥95%, Enzo Life Sciences, Inc., Lörrach, Germany) was dissolved in methanol (1 mg $mL^{-1}$). For the experiments, an aliquot of CYN dissolved in methanol was dried and re-dissolved in ultrapure water (UPW). Hydrogen peroxide (30%, w/w) was obtained from Acros Organics (Geel, Belgium). Tert-butanol (≥99.5%) was purchased from Merck KGaA (Darmstadt, Germany). Methanol (Rotisolv® HPLC Gradient), EtOH (Rotisolv® HPLC Gradient), and acetonitrile (Rotisolv® Ultra LC-MS grade) were obtained from Carl Roth (Karlsruhe, Germany). Formic acid was obtained from Fluka Analytical (Buchs, Switzerland). Sodium persulfate (≥98%), iron(II) sulfate heptahydrate (≥99%), silver sulfate (≥99.99%), and oxone® (2 $KHSO_5$ • $KHSO_4$ • $K_2SO_4$) were obtained from Sigma-Aldrich (Prague, Czech Republic). Cobalt(II) sulfate heptahydrate (≥99%) was purchased from VWR International (Leuven, Belgium). Human hepatocellular carcinoma (HCC) HepG2 (ATCC® HB-8065™) cells were purchased from LGC Standards (Łomianki, Poland). Other supplies were obtained from Sigma-Aldrich, if not specified otherwise.

### 2.2. CYN treatment

#### 2.2.1. CYN degradation pathways and residual toxicity

The potential degradation products were tentatively identified and the residual toxicity of treated CYN was assessed. Therefore, an initial CYN concentration of 10 μM was treated by 200 μM $Fe^{2+}$ and 100 μM $H_2O_2$ or 40 μM $Co^{2+}$ and 80 μM PMS. Metal and oxidant stock solutions were freshly produced at 5 mM in UPW. The ferrous iron stock solution was acidified with sulfuric acid to pH 2–3. The toxin was treated for 15 min at 20 ℃ in open amber glass vials. The reaction solutions reached pH values of approximately 3.1 and 4.2 for the Fenton and Fenton-like treatment without adjustment, respectively. Based on the optimization results (data shown in the Supplementary Information), CYN treatment by $Ag^{+}$/PS was too ineffective (Supplementary Information, Section 4.2.3) and was thus not further explored to investigate the degradation mechanisms and assessment of the residual toxicity.

Samples were taken before the reaction was initiated by adding the second reactant ($t_0$) and after 1, 2, 5, and 15 min. The reaction in the samples was quenched by excess concentrations of EtOH (approximately 160 mM). In order to evaluate the potential toxicity of the reaction mixture and to provide a corresponding solvent control for the toxicity assessments, blank Fenton and Fenton-like reaction solutions, i.e., without CYN, were also prepared in parallel, with the samples being collected before the initiation ($t_0$) and after 15 min of reaction. Subsequently, the samples were passed through a 0.22 μm cellulose acetate centrifugal filter at 7400g for 5 min and processed by solid-phase extraction (SPE) using graphitized carbon cartridges (S*Pure Extract-Clean SPE Carbograph, 500 mg/8 mL, S*Pure Pte Ltd, Singapore). The SPE procedure was adapted from (Triantis et al., 2016). In short, the SPE cartridges were conditioned with 10 mL of 80:20 dichloromethane: methanol acidified with 5% formic acid and rinsed with 10 mL UPW. Next, samples were loaded onto the cartridges. Then, the cartridges were washed with 60 mL UPW and air-dried for approximately 10 min. Residual CYN and degradation products were eluted using 15 mL of dichloromethane:methanol acidified with 5% formic acid.

After elution from the SPE cartridges, samples were dried under an $N_2$ stream at 45 ℃. Then, the dried samples were re-dissolved in 1 mL UPW and split into five aliquots, one for CYN quantification, one for degradation product identification, and three for residual toxicity assessment. The aliquots were again dried under an $N_2$ stream at 45 ℃. When necessary, the dried aliquots were frozen until usage. The dried aliquots were re-dissolved in UPW before the analysis or in the complete cell culture medium for the exposure of the hepatospheroids. In the in vitro assay, the final dilution of the AOP-treated samples with initially 10 μM CYN at $t_0$ was two-fold, i.e., 0.5-times the original CYN concentration, which corresponded to a final CYN concentration in the test of nominally 5 μM at $t_0$. In order to evaluate the potential effects of this SPE procedure on the CYN concentration and toxicity, a sample of untreated CYN (10 μM) was also filtered, loaded onto a conditioned SPE cartridge, eluted, re-dissolved, and diluted in the same way, i.e., to achieve a final concentration in the test nominally equivalent to 5 μM of CYN.

#### 2.2.2. Quenching experiments

The contribution of •OH and $SO_4^{-}$• to the degradation of CYN was investigated by treating the toxin under the same conditions as described for the degradation products identification and residual toxicity assessment in chapter 2.2.1 CYN degradation pathways and residual toxicity but this time, in the presence of either EtOH or tBuOH as radical quenchers. The quencher concentrations were adjusted according to a ratio of oxidant to quenching agent of 1:100. The sampling intervals were the same as before. The reaction in the samples was stopped by the addition of approximately 160 mM EtOH. The samples were passed through 0.22 μm cellulose acetate centrifugal filters at 7400*g* for 5 min and changes in the CYN concentration were analyzed by LC-DAD.

### 2.3. Analytical procedures

#### 2.3.1. CYN quantification

Cylindrospermopsin was quantified by an Agilent 1100 Infinity Series HPLC coupled with an Agilent 1100 Infinity Series DAD detector (Agilent Technologies Inc., Santa Clara, CA) at λ = 262 nm. Chromatographic separation was achieved on an InfinityLab Poroshell 120 SB-AQ column (3.0 × 100 mm, 2.7 μm, Agilent Technologies) equipped with an InfinityLab Poroshell 120 SB-AQ guard column (3.0 × 5 mm, 2.7 μm, Agilent Technologies) and gradient elution with acidified water (0.1% formic acid) and acidified acetonitrile (0.1% formic acid) (for details see Supplementary Table S1).

#### 2.3.2. Degradation product identification

Potential degradation products were characterized by HRMS (6550 Q-TOF, Agilent Technologies) coupled to an HPLC (1290 Infinity, Agilent Technologies). Samples were injected on a reversed-phase analytical column (BEH C18, 2.1 × 100 mm, 1.7 μm, Waters Corp., Milford, MA). A gradient elution program was used (for details, see Supplementary Table S2) with the mobile phase consisting of acidified water (0.1% formic acid) and acetonitrile (0.1% formic acid). Electrospray ionization was used in positive ion mode. The following mass spectrometry settings were used: gas temperature 200 ℃, gas flow 11 L $min^{-1}$, nebulizer pressure 40 psi, sheath gas temperature 320 ℃, sheath gas flow 10 L $min^{-1}$, capillary voltage 3500 V, fragmentor voltage 380 V, nozzle voltage 500 V, and a mass analyzer range of $m/z$ 100–600. If the detected peaks were also observed in the samples that were taken before the reaction was initiated ($t_0$), they were only considered to represent true product peaks if their peak area was at least twice the peak area in the sample taken at $t_0$ (adapted from Antoniou et al., 2008). $MS^2$ product ion scans were acquired at collision energies from 10 to 40 eV for structural confirmation of the identified degradation products shown in the proposed degradation pathways. The acquired data was processed using MassHunter Qualitative Analysis software (B.07.00, Agilent Technologies). The mass accuracy cut-off was kept at 10 ppm for precursor ions and at 20 ppm for product ions. All samples were analyzed in technical duplicates. The $MS^2$ spectra of CYN and the degradation products included in the proposed degradation pathways are shown in the Supplementary Figs. S8–S53. A compound structure was confirmed by $MS^2$, detecting at least one product ion at high relative intensity

identified based on literature or $MS^2$ spectra interpretation.

### 2.3.3. Toxicity assessment

For the assessment of the residual toxicity of treated CYN and its degradation products, the cytotoxicity to 14 days old HepG2 cell spheroids was evaluated. A detailed description of the cell cultivation, spheroid preparation, and toxicity assays can be found in the Supplementary Information. Briefly, the spheroids were prepared by seeding HepG2 cells (1000 cells per well) into 96-well microplates with the well bottom pre-coated with 1.5% agarose, which resulted in cell aggregation producing a single spheroid per well. Before the assay, HepG2 spheroids were incubated for 14 days to improve their hepatocyte-specific differentiation, as previously reported by Gaskell et al. (2016) and Kim et al. (2019). Before the experiments, the spheroid size and morphology were evaluated by Cytation 5 MFV brightfield imaging using a 4× objective and Gen5 software (BioTek, Winooski, VT). Spheroid treatment started after replacing 100 µL of the culture media in the well with the tested samples pre-diluted in the culture medium. Non-treated (naïve) control spheroids were exposed to culture medium only. Corresponding solvent controls were conducted in each experiment, using either UPW (1% water in culture media, v/v) for the assessment of the concentration-response relationship for untreated CYN, or samples from blank Fenton and Fenton-like reaction solutions without CYN (after 0 and 15 min) for the toxicity assessment of CYN degradation. A high concentration (10%, v/v) of dimethyl sulfoxide (DMSO) was used as a positive control. For the degradation experiments, untreated CYN was also used as a positive control (at 5 µM final nominal concentration in the well), including both (1) untreated CYN diluted in the culture media and (2) untreated CYN processed through the same SPE procedure as the samples of AOP-treated CYN. Agarose-coated wells without spheroids were used as blanks for resazurin and ATP assays. The spheroids were exposed for 96 h at 37 ℃ and under 5% $CO_2$.

After the exposure, spheroid size and morphology were again documented by Cytation 5 MFV. Subsequently, the effects of CYN and its degradation products were first determined by reducing resazurin to resorufin, which mainly depends on the activity of NAD(P)H-dehydrogenases (oxidoreductases) of the viable cells. Therefore, the spheroids were rinsed with phosphate-buffered saline (PBS) and incubated for 2 h (37 ℃, 5% $CO_2$) with resazurin. The fluorescence of resorufin was then measured at 560 nm (excitation) and 590 nm (emission) using a SynergyMX (BioTek). Next, the ATP content, proportional to the number of viable and metabolically active cells in the spheroid, was determined by CellTiter-Glo® 3D Cell Viability Assay (Promega, Madison, WI). In brief, the spheroids were rinsed again with PBS, and then the CellTiter-Glo® 3D Reagent was added to each well to facilitate ATP release and provide reagents for the subsequent ATP-dependent luminescent reaction. The plate was vigorously mixed for 5 min and incubated for 25 min at room temperature. The luminescence was then recorded using a SpectraMax luminometer (Molecular Devices, LLC, San Jose, CA).

All exposure treatments were prepared in triplicates, i.e., three microplate wells per sample, and each experiment was repeated three times independently, i.e., on three different microplates. The spheroid size is reported as diameter (in µm), as well as relative spheroid growth, i.e., the change of the spheroid size during the exposure relative to the growth of non-treated spheroids (naïve control) from the same plate (expressed as % control). For the resazurin and ATP assays, assay blank-subtracted fluorescence or luminescence values were compared to the average values of the naïve controls from the same plate (expressed as % control). For the statistical data analysis, values derived from independent experiments ($n \geq 3$) were used.

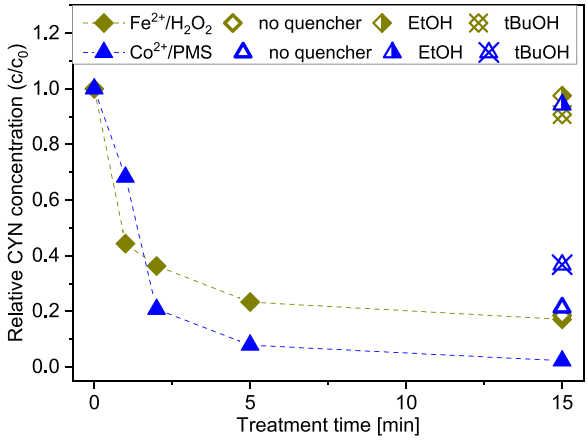


**Fig. 1.** CYN removal (initial concentration 10 µM) by two treatments (200 µM $Fe^{2+}$/100 µM $H_2O_2$ and 40 µM $Co^{2+}$/80 µM PMS) after 15 min of treatment at 20 °C. The effects of two radical quenchers (EtOH and tBuOH) on the CYN removal by $Fe^{2+}/H_2O_2$ and $Co^{2+}$/PMS after 15 min is also shown.

## 3. Results and discussion

### 3.1. CYN degradation

In order to tentatively identify degradation products and assess the residual toxicity after the treatment, an initial CYN concentration of 10 µM was treated by $Fe^{2+}/H_2O_2$ and $Co^{2+}$/PMS for 15 min at CYN to metal ratios of 0.05:1 and 0.25:1, respectively. These treatment conditions were adapted from the optimization study shown in the Supplementary Information.

Fig. 1 shows the degradation of CYN by $Fe^{2+}/H_2O_2$ and $Co^{2+}$/PMS under adjusted reaction conditions and its degradation in the presence of radical quenchers. Both degradation reactions followed a second-order reaction. However, degradation by the Fenton-like reaction appeared to be more effective as 98% of the toxin were degraded after 15 min of treatment while the Fenton reaction achieved 83% degradation (Fig. 1), even though the CYN to metal ratio was five times lower for the Fenton reaction, i.e., higher reagent concentrations.

The $Co^{2+}$/PMS treatment could have been more effective than $Fe^{2+}/H_2O_2$ because i) the Fenton-like reaction produced the reactive species more efficiently, i.e., in higher quantity, and ii) the produced $SO_4^{\bullet-}$ was more reactive than •OH as indicated by their redox potentials of 2.5–3.1 V/SHE for $SO_4^{\bullet-}$ and 2.7 V/SHE for •OH under acidic and neutral conditions (Schneider and Bláha, 2020).

Regarding the experimental conditions, CYN degradation by the Fenton reaction is assumed to be driven by •OH while the Fenton-like reaction may generate SO4-• and •OH simultaneously, which could contribute to the degradation. Hence, for a better understanding and comparison of the underlying degradation mechanisms, the treatments were repeated in the presence of the two radical quenchers EtOH and tBuOH. Due to rate constants of EtOH with •OH and $SO_4^{\bullet-}$ in the range of $10^9$ $M^{-1}s^{-1}$ and $10^7$ $M^{-1}s^{-1}$ (Verma et al., 2016), respectively, it was considered to be a suitable quenching agent for both radicals. Conversely, the rate constants for the reaction of tBuOH with •OH and $SO_4^{\bullet-}$ are in the range of $10^8$ $M^{-1}s^{-1}$ and $10^5$ $M^{-1}s^{-1}$ (Verma et al., 2016), respectively, and it thus quenches •OH more effectively than $SO_4^{\bullet-}$. CYN degradation by the Fenton reaction decreased to 2% in the presence of EtOH and to 9% in the presence of tBuOH (Fig. 1). Ethanol is a slightly more effective •OH quencher than tBuOH but, as expected, both quenching agents effectively inhibited the degradation by the Fenton reaction. This indicated that the CYN degradation by the Fenton reaction was primarily driven by •OH.

In contrast, the CYN degradation by the Fenton-like reaction was reduced to 6% in the presence of EtOH and to 63% in the presence of tBuOH (Fig. 1). Hence, the inhibition of the CYN degradation by the Fenton-like reaction was substantially less effective in the presence of tBuOH. As tBuOH quenches •OH more effectively than $SO_4^{\bullet-}$, these results indicated that the CYN degradation by the Fenton-like reaction was

**Table 1**
List of degradation products observed after treatment by either $Co^{2+}$/PMS or $Fe^{2+}/H_2O_2$ (products in [brackets] were not confirmed by $MS^2$). This list only shows the products depicted in Figs. 2–7. A more extensive list with all observed degradation products and further information can be found in Supplementary Table S3.

| Product name | m/z | Chemical formula | Observed after treatment by | | Shown in the proposed reaction scheme |
|---|---|---|---|---|---|
| | | | $Co^{2+}$/PMS | $Fe^{2+}/H_2O_2$ | |
| CYN | 416.1252 | $C_{15}H_{21}N_5O_7S$ | – | – | uracil, guanidine, sulfate |
| [195] | 195.1367 | $C_{10}H_{16}N_3O$ | ✓ | × | uracil |
| [210] | 210.1231 | $C_{10}H_{15}N_3O_2$ | ✓ | ✓ | uracil |
| [214b] | 214.1200 | $C_9H_{15}N_3O_3$ | ✓ | × | uracil |
| 224a | 224.1041 | $C_{10}H_{13}N_3O_3$ | ✓ | ✓ | uracil |
| 226 | 226.1195 | $C_{10}H_{15}N_3O_3$ | ✓ | ✓ | uracil |
| 240b | 240.1357 | $C_{11}H_{17}N_3O_3$ | ✓ | ✓ | uracil |
| 242b | 242.1147 | $C_{10}H_{15}N_3O_4$ | ✓ | ✓ | uracil |
| 290a | 290.0818 | $C_{10}H_{15}N_3O_5S$ | ✓ | ✓ | uracil |
| 292 | 292.0972 | $C_{10}H_{17}N_3O_5S$ | × | ✓ | uracil |
| 304b | 304.0978 | $C_{11}H_{17}N_3O_5S$ | ✓ | ✓ | uracil |
| 306 | 306.0768 | $C_{10}H_{15}N_3O_6S$ | ✓ | ✓ | uracil |
| 308b | 308.0929 | $C_{10}H_{17}N_3O_6S$ | ✓ | ✓ | uracil |
| 320a | 320.0924 | $C_{11}H_{17}N_3O_6S$ | ✓ | ✓ | uracil |
| 322b | 322.1082 | $C_{11}H_{19}N_3O_6S$ | ✓ | ✓ | uracil |
| 334a | 334.0713 | $C_{11}H_{15}N_3O_7S$ | ✓ | ✓ | uracil |
| 334b | 334.1524 | $C_{15}H_{19}N_5O_4$ | ✓ | ✓ | sulfate |
| 336 | 336.0894 | $C_{11}H_{17}N_3O_7S$ | ✓ | ✓ | uracil |
| 338a | 338.1038 | $C_{11}H_{19}N_3O_7S$ | ✓ | ✓ | uracil |
| 338b | 338.1475 | $C_{14}H_{19}N_5O_5$ | ✓ | ✓ | guanidine |
| 349 | 349.1190 | $C_{12}H_{20}N_4O_6S$ | ✓ | × | uracil |
| 350a | 350.1031 | $C_{12}H_{19}N_3O_7S$ | ✓ | ✓ | uracil |
| 350b | 350.1473 | $C_{15}H_{19}N_5O_5$ | ✓ | ✓ | sulfate |
| 366a | 366.0979 | $C_{12}H_{19}N_3O_8S$ | ✓ | × | uracil |
| 373 | 373.0827 | $C_{13}H_{16}N_4O_7S$ | ✓ | × | uracil |
| 375 | 375.0984 | $C_{13}H_{18}N_4O_7S$ | ✓ | ✓ | uracil |
| [382b] | 382.1370 | $C_{15}H_{19}N_5O_7$ | ✓ | ✓ | sulfate |
| 384 | 384.1526 | $C_{15}H_{21}N_5O_7$ | ✓ | ✓ | guanidine, sulfate |
| 391 | 391.0934 | $C_{13}H_{18}N_4O_8S$ | ✓ | ✓ | uracil |
| 392 | 392.1243 | $C_{13}H_{21}N_5O_7S$ | ✓ | ✓ | uracil |
| [398] | 398.1315 | $C_{15}H_{19}N_5O_8$ | ✓ | ✓ | sulfate |
| 405 | 405.0727 | $C_{13}H_{16}N_4O_9S$ | ✓ | × | uracil |
| 407 | 407.0887 | $C_{13}H_{18}N_4O_9S$ | ✓ | × | uracil |
| 414 | 414.1091 | $C_{15}H_{19}N_5O_7S$ | ✓ | ✓ | uracil, guanidine |
| [418] | 418.1046 | $C_{14}H_{19}N_5O_8S$ | ✓ | × | guanidine |
| 420 | 420.1199 | $C_{14}H_{21}N_5O_8S$ | ✓ | ✓ | uracil |
| 430 | 430.1037 | $C_{15}H_{19}N_5O_8S$ | ✓ | ✓ | uracil, guanidine |
| 432 | 432.1196 | $C_{15}H_{21}N_5O_8S$ | ✓ | × | uracil, guanidine, sulfate |
| 436 | 436.1140 | $C_{14}H_{21}N_5O_9S$ | ✓ | × | uracil |
| 446 | 446.0994 | $C_{15}H_{19}N_5O_9S$ | ✓ | ✓ | uracil |
| 448 | 448.1146 | $C_{15}H_{21}N_5O_9S$ | ✓ | ✓ | uracil, guanidine |
| 450 | 450.1298 | $C_{15}H_{23}N_5O_9S$ | × | ✓ | uracil |
| 452 | 452.1096 | $C_{14}H_{21}N_5O_{10}S$ | ✓ | × | uracil |
| 464 | 464.1097 | $C_{15}H_{21}N_5O_{10}S$ | ✓ | ✓ | uracil, guanidine |
| 480 | 480.1048 | $C_{15}H_{21}N_5O_{11}S$ | ✓ | ✓ | guanidine |
| 496 | 496.0999 | $C_{15}H_{21}N_5O_{12}S$ | ✓ | × | guanidine |

mainly driven by $SO_4^{\bullet-}$ while the contribution of •OH was substantially lower. When assuming that •OH and $SO_4^{\bullet-}$ are the only reactive species produced by the Fenton-like reaction that contributed to the degradation of CYN, the 63% degradation in the presence of tBuOH would correspond to a contribution of the $SO_4^{\bullet-}$ of about 80% to the overall CYN degradation. Although tBuOH quenched $SO_4^{\bullet-}$ less effectively than •OH, it assumingly still reduced the $SO_4^{\bullet-}$-driven CYN degradation to an unknown degree. Therefore, this 80% of the contribution of $SO_4^{\bullet-}$ to the overall CYN degradation most likely underestimates the true value, i.e. the contribution to the degradation caused by $SO_4^{\bullet-}$ might be even higher.

### 3.1.1. CYN degradation pathways

Samples from the treatment by $Co^{2+}$/PMS and $Fe^{2+}/H_2O_2$ were screened for potential degradation products using ToF-HRMS. We set up an instrument method with an inclusion list containing 180 previously reported CYN degradation products (Adamski et al., 2016b, 2016a; Chen et al., 2015; Fotiou et al., 2015; He et al., 2014b; León et al., 2019; Liu et al., 2018; Martínez-Ruiz et al., 2020; Merel et al., 2010; Song et al., 2012; Wang et al., 2014; Wu et al., 2015; Yan et al., 2016; Zhang et al., 2015b). Refer to Supplementary Table S3 for the complete list of products. We detected 165 previously reported degradation products in our experiments. Following the blank subtraction, 116 product peaks remained. Table 1 lists the tentatively identified products included in the proposed degradation pathways and shows in which treatment they were observed. The tentative structures (Table 1) were further validated using QToF-$MS^2$. Detected $MS^2$ fragments are compiled in Supplementary Table S3. The time profiles of degradation products listed in Table 1 are shown in the Supplementary Figs. S54-S59.

The hydroxymethyl uracil moiety, the tricyclic guanidine system and the sulfate group were identified as susceptible moieties for the degradation by $SO_4^{\bullet-}$ and •OH. Therefore, the discussion of the proposed degradation pathways was separated in the three sub-chapters: 3.1.1.1 Attack at the hydroxymethyl uracil moiety and subsequent fragmentation, 3.1.1.2 Attack at the tricyclic guanidine, and 3.1.1.3 Attack at the sulfate group. The last column in Table 1 shows in which proposed degradation pathway scheme the respective degradation product is depicted.

*3.1.1.1. Attack at the hydroxymethyl uracil moiety and subsequent fragmentation.* The proposed degradation pathway for the first part of the attack and subsequent ring cleavage of the hydroxymethyl uracil moiety is shown in Fig. 2. In agreement with other studies (He et al., 2014b), the C═C double bond was the dominant target for mono- and dihydroxylation reactions at the hydroxymethyl uracil moiety of the parent toxin, which led to the formation of *m/z = 432* and *450*, respectively. Although *m/z = 432* was only observed for the $SO_4^{\bullet-}$-based treatment while *m/z = 450* was only observed for the •OH-based treatment, their respective dehydrogenated products *m/z = 430* and *448* were observed for both treatments (Table 1). Besides dehydrogenation of *m/z = 432*, *m/z = 430* could also be formed by hydroxylation of *m/z = 414,* which is the dehydrogenated product of CYN. In fact, for both treatments, *m/z = 414* was more abundant than *m/z = 430* (Supplementary Fig. S54). Although *m/z = 448* is often detected in other studies, *m/z = 450* has so far only been reported by Fotiou et al. (2015). This could indicate that *m/z = 450* is a transient intermediate product that is readily oxidized to *m/z = 448*. The degradation product time profiles appeared to confirm this assumption as higher quantities of *m/z = 448* than *m/z = 450* were detected (Supplementary Fig. S54). Moreover, *m/z = 448* was the most abundant product formed by the $SO_4^{\bullet-}$-based treatment (Supplementary Figs. S54-S59), indicating that the dihydroxylation of CYN was a crucial reaction step. Contrarily, for the •OH-based treatment, *m/z = 448* was less abundant, especially in the first 2 min of the treatment (Supplementary Fig. S54). Following another hydroxylation and consequential uracil ring cleavage in *m/z = 464*, *m/z = 420* was formed by decarboxylation. From there, the product could either be further oxidized in a stepwise hydroxylation to form the products *m/z = 436* and *452*, or it could be further fragmented to form *m/z = 392*. Interestingly, the hydroxylated products *m/z = 436* and *452* were only observed for the $SO_4^{\bullet-}$-based treatment. Following the loss of the terminal amide nitrogen of the urea moiety in *m/z = 392*, ring formation led to *m/z = 375*. In a subsequent step, the carbonyl group was removed to form *m/z = 349,* which was only observed for the $SO_4^{\bullet-}$-based treatment and seemed to only be a transient product

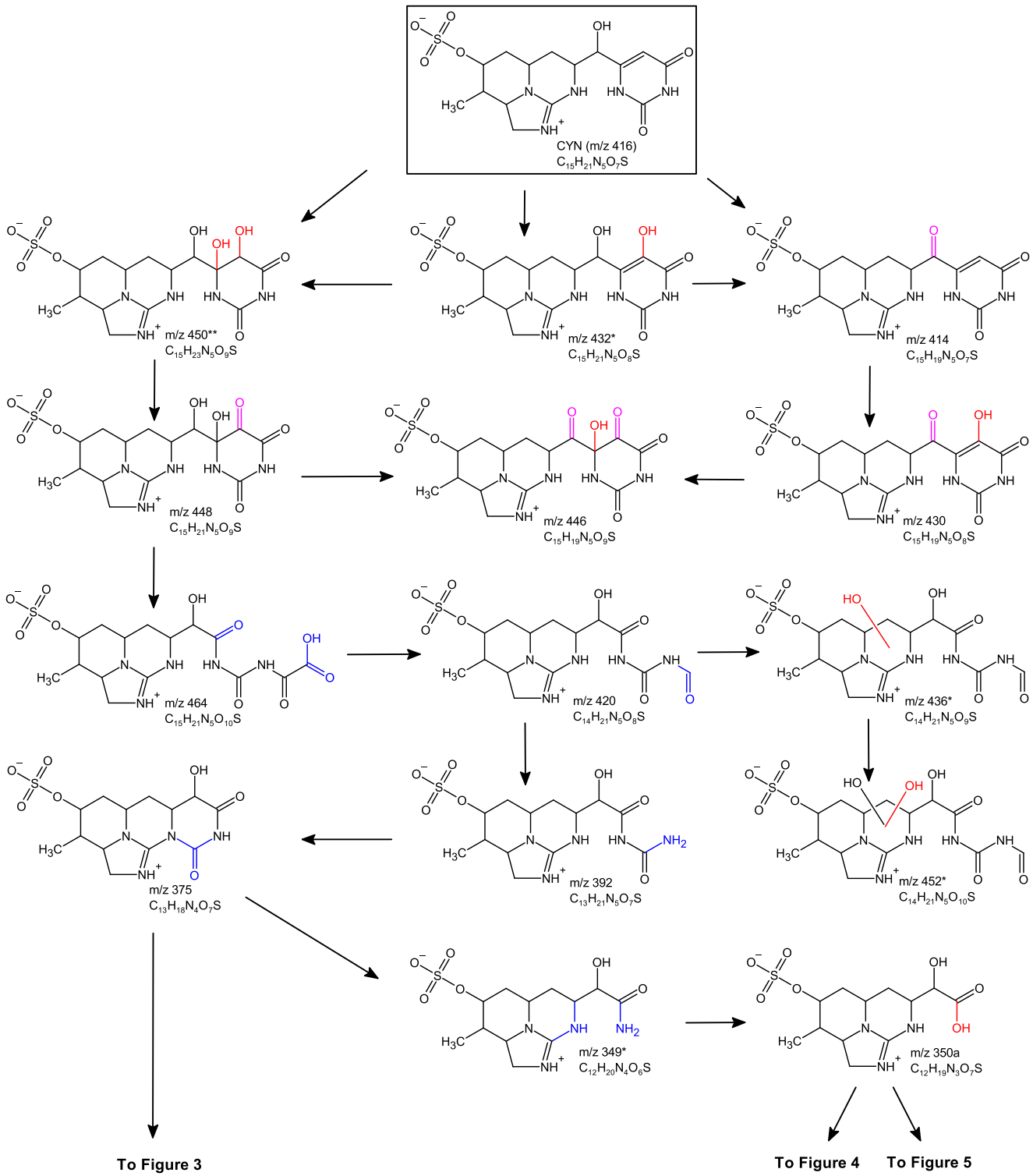


**Fig. 2.** First part of the proposed CYN degradation pathway for the primary attack at the hydroxymethyl uracil moiety with subsequent uracil ring cleavage. Colors indicate the dominant degradation process: hydroxylation, dehydrogenation, and fragmentation and ring cleavage (readers are referred to the online version of this article). Products marked with asterisks were only observed after "*" $Co^{2+}$/PMS or "**" $Fe^{2+}/H_2O_2$ treatment. For interpretation of the references to color in this figure legend, the reader is referred to the web version of this article.

(Supplementary Fig. S54). Loss of the amide nitrogen and hydroxylation led to the formation of *m/z = 350a*, which is often referred to as *cylindrospermopsic acid* (He et al., 2014b; Yan et al., 2016). Interestingly, for the $Co^{2+}$/PMS treatment, *m/z = 375* was more abundant than *m/z = 350a* while it was the opposite for the $Fe^{2+}/H_2O_2$ treatment (Supplementary Fig. S54).

Fig. 3 continues the proposed degradation pathway focusing on the oxidation of the tricyclic guanidine system starting from the product *m/z = 375*. This product could either be dehydrogenated to form *m/z = 373* or it could be further hydroxylated at three different position at the tricyclic guanidine system to form *m/z = 391*, i.e. the tertiary amine or at two different methylene groups which was then followed by

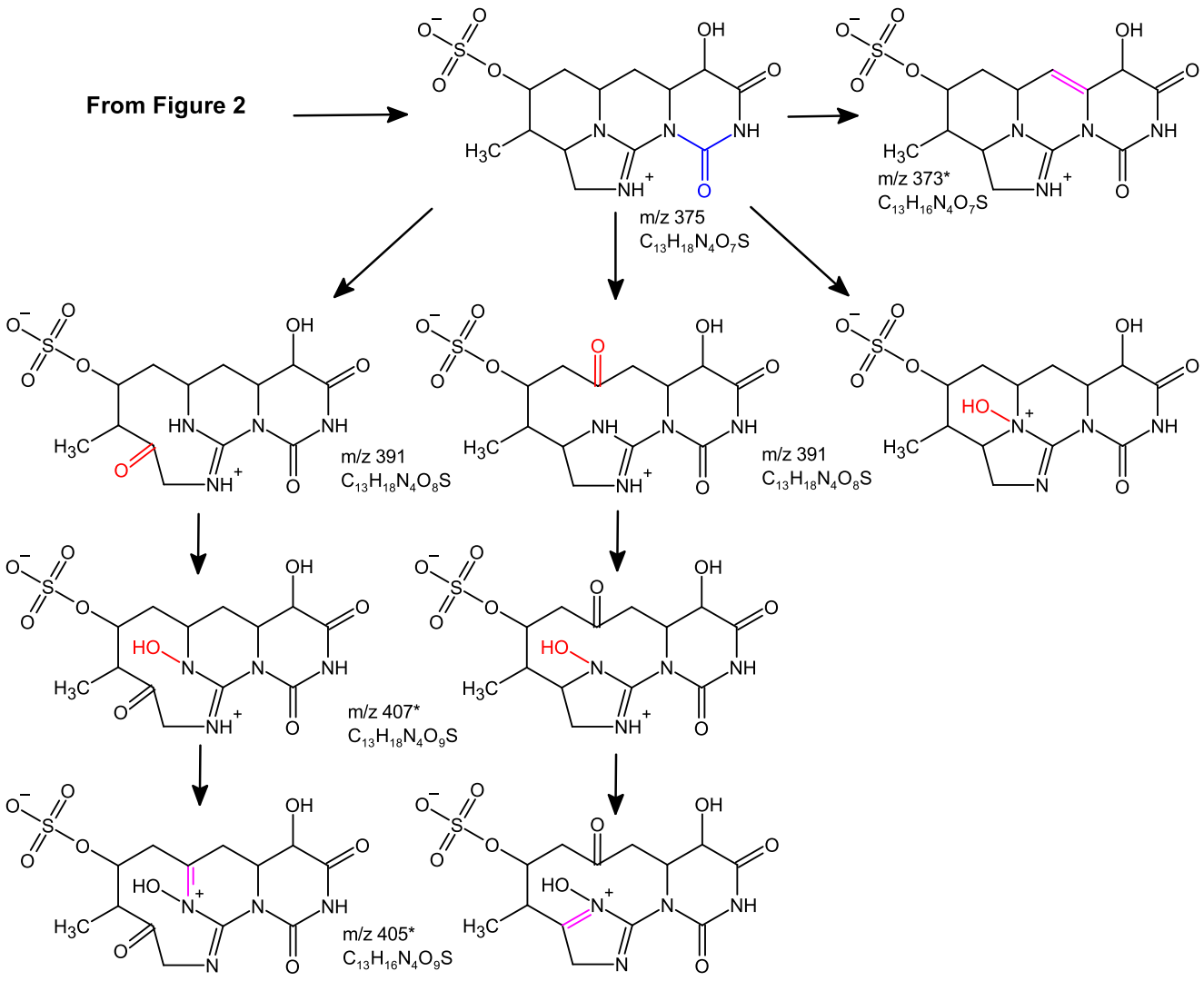


**Fig. 3.** Second part of the proposed CYN degradation pathway for the primary attack at the hydroxymethyl uracil moiety continuing by oxidation of the tricyclic guanidine system, starting from *m/z = 375*. Colors indicate the dominant degradation process: hydroxylation and dehydrogenation (readers are referred to the online version of this article). Products marked with asterisks were only observed after "* " $Co^{2+}$/PMS treatment. For interpretation of the references to color in this figure legend, the reader is referred to the web version of this article.

dehydrogenation. The two products with *m/z = 391* that were not hydroxylated at the tertiary amine could then be hydroxylated in this position to form *m/z = 407* which was then dehydrogenated to form *m/z = 405*. The products with *m/z = 373*, *405* and *407* were only observed after treatment by $Co^{2+}$/PMS. The reason for this could have been the abundance of the *m/z = 375* which was substantially higher for the $SO_4^{\bullet-}$- than for the •OH-based treatment (Supplementary Fig. S55).

Fig. 4 continues to show the degradation pathway starting from product *m/z = 350a*, which included further fragmentation of the hydroxymethyl uracil moiety and oxidation of the tricyclic guanidine system. Like *m/z = 375*, *m/z = 350a* could be hydroxylated at the tertiary amine or two different methylene groups for which the reaction included subsequent dehydrogenation to form *m/z = 366a*. Following, *m/z = 322b* was formed by decarboxylation of the carboxylic acid group. Although *m/z = 366a* was only formed by the reaction of *m/z = 350a* with $SO_4^{\bullet-}$, *m/z = 322b* was again observed for both treatments. After oxidation of the hydroxymethyl group in *m/z = 322b* with the hydroxylated tertiary amine to an aldehyde (*m/z = 320a*), *m/z = 292* was then formed by removal of the aldehyde group. Interestingly, this product was only observed after treatment by $Fe^{2+}/H_2O_2$. He et al. (2014a) did detect a product with *m/z = 292* after degradation of CYN by $SO_4^{\bullet-}$ but they only proposed a structure with the hydroxylation at a methylene group (as shown Fig. 5) in their related publication (He et al., 2014b). Contrarily, the proposed structure for *m/z = 292* with the hydroxyl group at the tertiary amine was based on Yan et al. (2016), who observed both forms of *m/z = 292*. Although we only detected one peak corresponding to *m/z = 292*, the chromatographic separation of these two products may simply not have been as good in our study. For the two possible forms of *m/z = 322b* with the ketone group, degradation could have continued via hydroxylation of the tertiary amine (*m/z = 338a*), dehydrogenation of the hydroxymethyl group (*m/z = 336*) and subsequently, removal of the aldehyde moiety (*m/z = 308b*). Two other possible forms of *m/z = 336* could have also been formed directly from *m/z = 322b* by hydroxylation of the tertiary amine and subsequent dehydrogenation. However, a higher abundance of *m/z = 338a* compared with *m/z = 320a* and *m/z = 336* showed that the production of this intermediate was more pronounced and thus, indicated that it was the preferred reaction pathway, especially for the •OH-based treatment (Supplementary Fig. S56). The oxidation of the hydroxymethyl group to an aldehyde in *m/z = 336* produced *m/z = 334a*. Removal of the aldehyde in *m/z = 334a* led to the formation of *m/z = 306*.

Fig. 5 shows the further degradation of *m/z = 350a* including removal of the residual part of the hydroxymethyl uracil moiety and

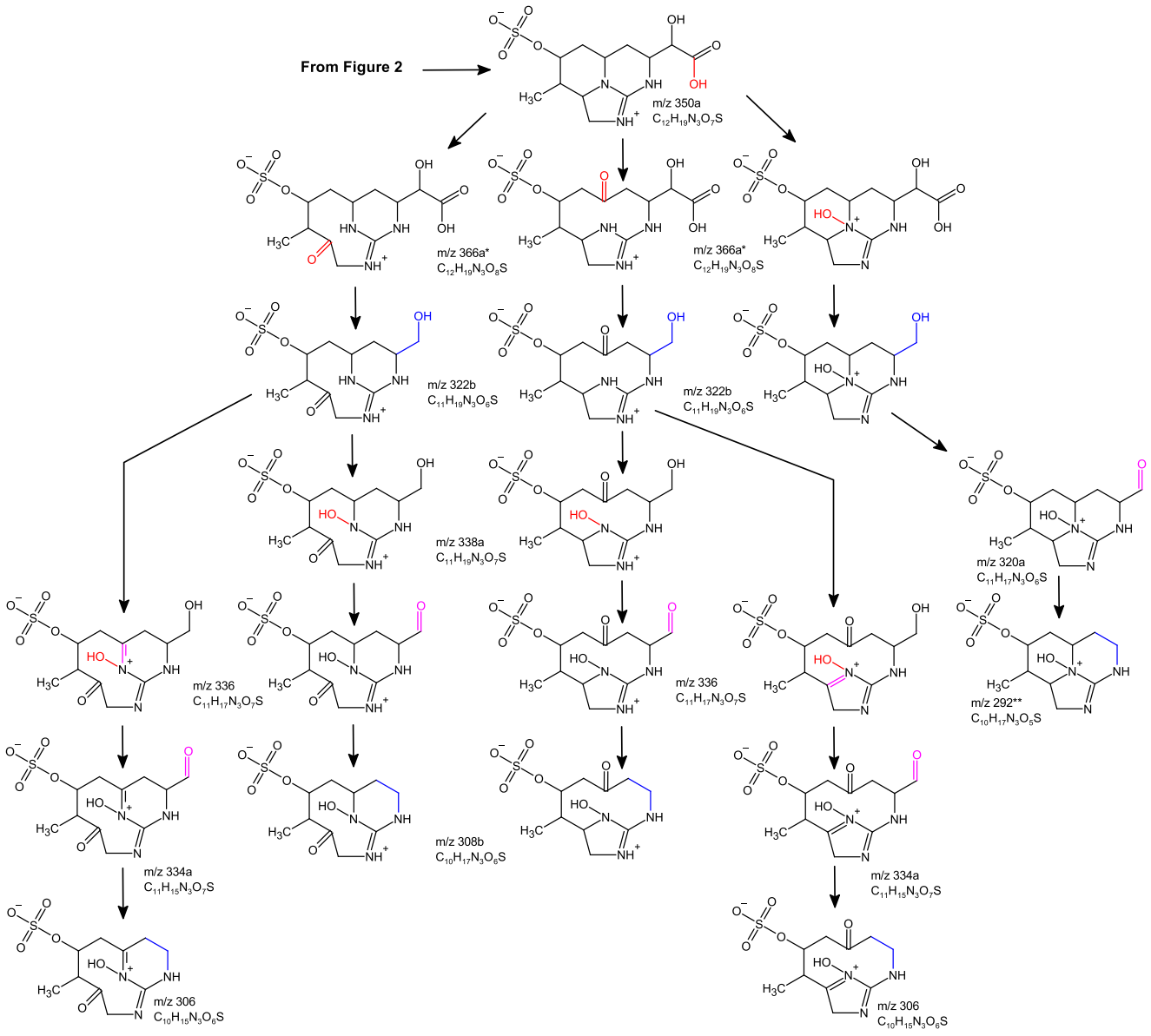


**Fig. 4.** Third part of the proposed CYN degradation pathway for the primary attack at and removal of the residual of the hydroxymethyl uracil moiety continuing from *m/z = 350a*. Colors indicate the dominant degradation process: hydroxylation, dehydrogenation, and fragmentation (readers are referred to the online version of this article). Products marked with asterisks were only observed after "* " $Co^{2+}$/PMS or "* *" $Fe^{2+}$/$H_2O_2$ treatment. For interpretation of the references to color in this figure legend, the reader is referred to the web version of this article.

sulfate group as well as cleavage of the tricyclic guanidine system. The product *m/z = 304b* is formed via sequential decarboxylation of the carboxylic acid group and dehydrogenation of the remaining hydroxymethyl group in *m/z = 350a*. The aldehyde in *m/z = 304b* was then further oxidized to a carboxylic acid (*m/z = 320a*) via hydration (*m/z = 322b*). Decarboxylation-hydroxylation then led to the formation of the other possible form of *m/z = 292*, which could be further oxidized either to another form of *m/z = 308b* via hydroxylation in 1,2-position to the other hydroxyl group or to *m/z = 290a* via oxidation of the hydroxyl group to an aldehyde. Instead of being degraded to *m/z = 292*, *m/z = 320a* could also be degraded by removing the sulfate group (*m/z = 240b*). Decarboxylation of the carboxylic acid in *m/z = 240b* and subsequent dehydrogenation led to the formation of an aldimine (*m/z = 195*), which was only observed for treatment by $SO_4^{-}$•. Contrarily, this product was so far only detected by Fotiou et al. (2015) after $TiO_2$-based photocatalytic treatment by UV-A and solar light, i.e., in the absence of $SO_4^{-}$•. This strengthened the assumption that for both treatments, although driven by different radicals, the degradation mechanisms were similar and, consequentially, resulted in the formation of the same degradation products. Instead of forming the aldimine after removing the carboxylic acid group in *m/z = 240b*, this position could also be subjected to hydroxylation-dehydrogenation, which was one of the possible pathways for the formation of *m/z = 210*. The other possible pathway was the removal of the sulfate group in *m/z = 290a*. The degradation pathway via *m/z* = 290a appeared to be more pronounced for both treatments compared with the pathway via *m/z = 240b* (Supplementary Fig. S57), indicating that the decarboxylation was preferred over sulfate group removal from *m/z = 320a*. The product *m/z = 210* was then hydroxylated in 1,2-position to the amide carbonyl group (*m/z = 226*) and further oxidized to form the 1,2-diketone (*m/z = 224a*). Product *m/z = 242b* was then formed by ring cleavage at the amide group and oxidation of the 1,2-ketone to a keto acid. A carboxylic acid then replaced this keto acid via decarboxylation-hydroxylation (*m/z = 214b*).

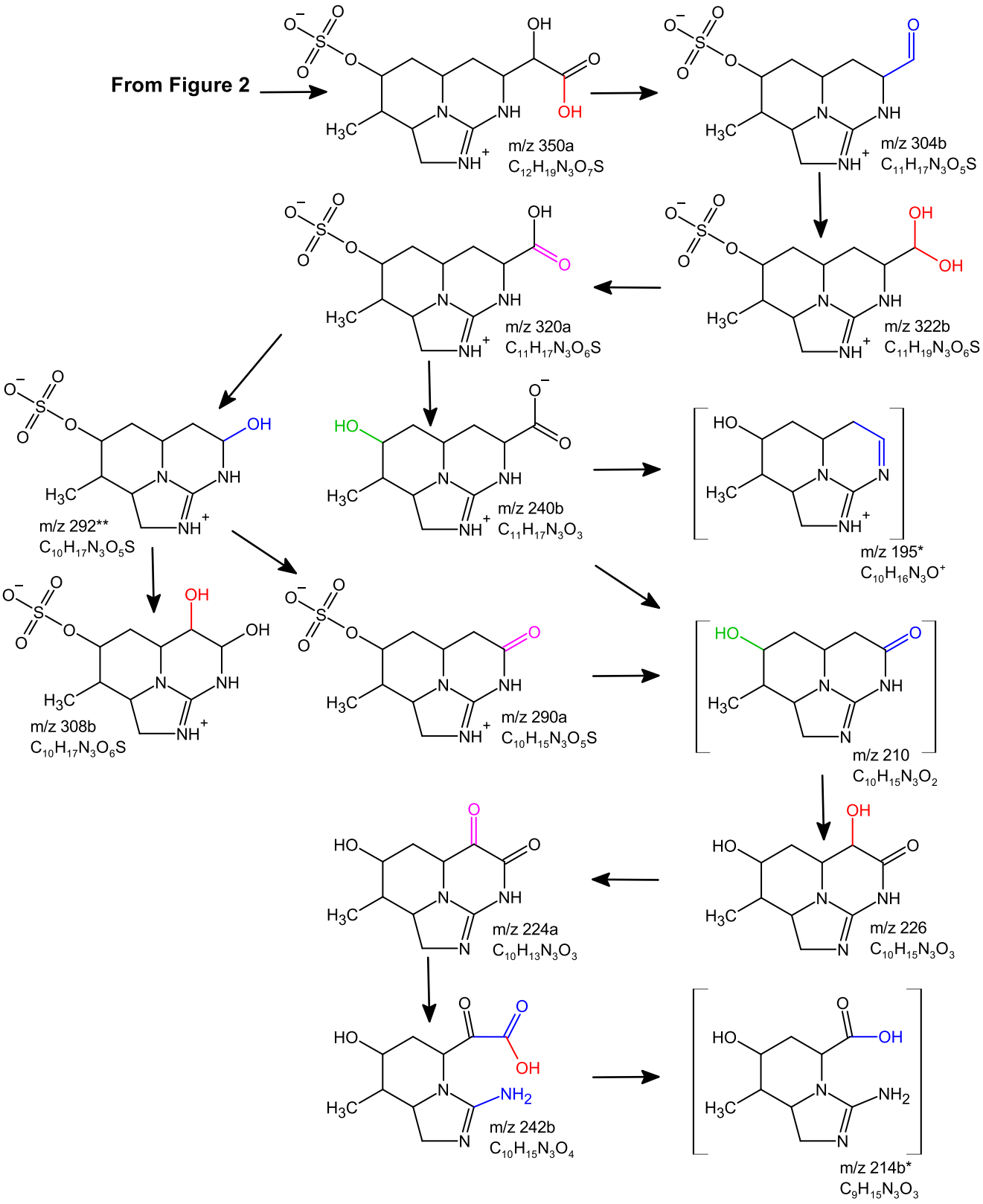


**Fig. 5.** Fourth part of the proposed CYN degradation pathway for the primary attack at and removal of the residual of the hydroxymethyl uracil moiety and subsequent removal of the sulfate group and ring cleavage of the tricyclic guanidine structure continuing from *m/z = 350a*. Colors indicate the dominant degradation process: hydroxylation, dehydrogenation, sulfate group removal, and fragmentation and ring cleavage (readers are referred to the online version of this article). Products in [brackets] were not confirmed by $MS^2$. Products marked with asterisks were only observed after "*" $Co^{2+}$/PMS or "**" $Fe^{2+}/H_2O_2$ treatment. For interpretation of the references to color in this figure legend, the reader is referred to the web version of this article.

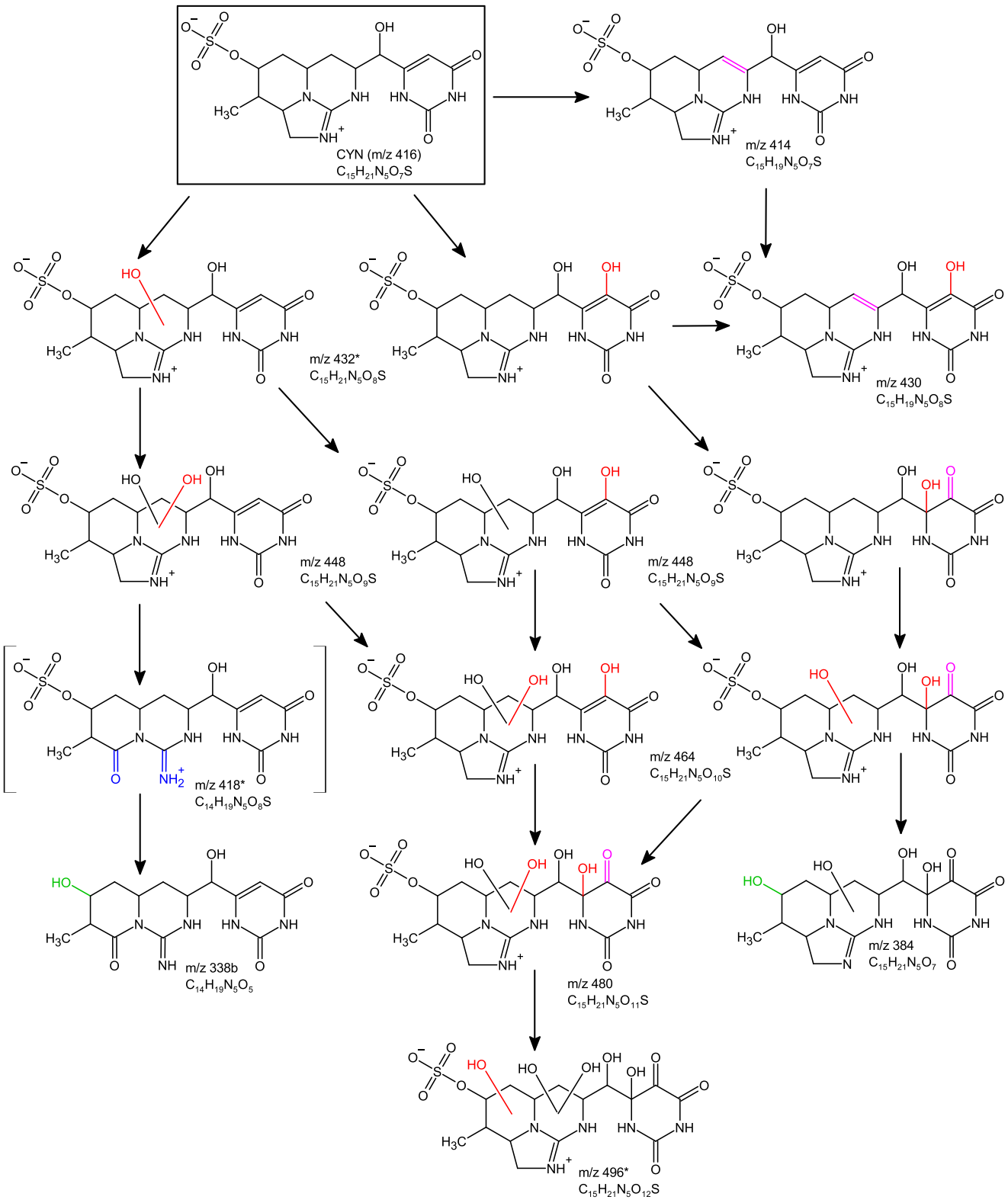


**Fig. 6.** Proposed CYN degradation pathway for the primary attack at the tricyclic guanidine structure with subsequent sulfate group removal and ring cleavage. Colors indicate the dominant degradation process: hydroxylation, dehydrogenation, sulfate group removal, and fragmentation and ring cleavage (readers are referred to the online version of this article). Products in [brackets] were not confirmed by $MS^2$. Products marked with asterisks were only observed after "*" $Co^{2+}$/PMS treatment. For interpretation of the references to color in this figure legend, the reader is referred to the web version of this article.

*3.1.1.2. Attack at the tricyclic guanidine.* Fig. 6 shows the proposed degradation pathway following attacks primarily at the tricyclic guanidine system, which involved sequential hydroxylation, dehydrogenation, ring cleavage, and removing the sulfate group. Conversely to the form of $m/z = 414$ shown in Fig. 2, CYN could also be dehydrogenated at the tricyclic system. Besides that, the parent toxin was hydroxylated at different positions, i.e., at the C=C double bond in the hydroxymethyl uracil group and at different positions in the tricyclic guanidine structure. Monohydroxylation of CYN led to the formation of two possible forms of $m/z = 432$, which could be further hydroxylated to three forms of $m/z = 448$. The product $m/z = 430$ was produced either by hydroxylation of $m/z = 414$ or dehydrogenation of $m/z = 432$. Further stepwise hydroxylation of $m/z = 448$ led to the formation of two other forms of $m/z = 464$ (in contrast to sequential trihydroxylation at the hydroxymethyl uracil moiety as shown in Fig. 2), $m/z = 480$, and $m/z = 496$. The two products $m/z = 432$ and $m/z = 496$ were only observed for the $SO_4^{-}$•-based treatment. However, both products have previously been reported to be produced by •OH-based AOPs as well (He et al., 2014b). According to their detected quantities, $m/z = 448$ was the most abundant product for this part of the degradation pathway for the treatment by $Co^{2+}$/PMS, followed by $m/z = 480$ whose production substantially increased after 1 min of treatment (Supplementary Fig. S58). In contrast, $m/z = 414$ was the primary product in the first 2 min of treatment by $Fe^{2+}/H_2O_2$, before $m/z = 448$ production increased while $m/z = 480$ was only produced in very low quantities (Supplementary Fig. S58). This indicated that the $SO_4^{-}$•-based treatment preferably started the degradation by hydroxylation reactions while the less selective •OH apparently first primarily reacted with the parent toxin by

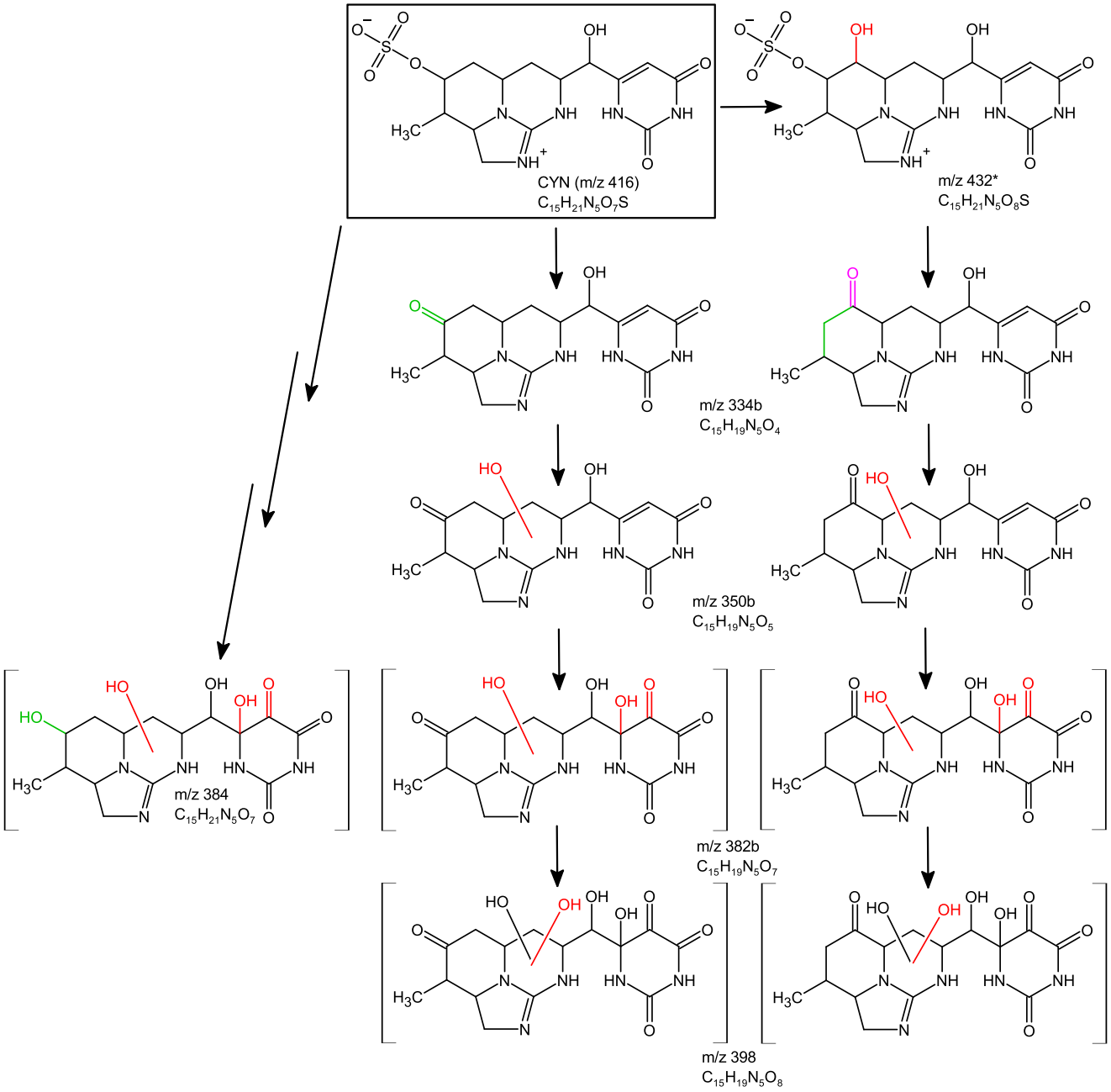


**Fig. 7.** Proposed CYN degradation pathway for the primary attack at the sulfate group with subsequent hydroxylation. Colors indicate the dominant degradation process: hydroxylation, dehydrogenation, and sulfate group removal (readers are referred to the online version of this article). Products in [brackets] were not confirmed by $MS^2$. Products marked with asterisks were only observed after "*" $Co^{2+}$/PMS treatment. For interpretation of the references to color in this figure legend, the reader is referred to the web version of this article.

dehydrogenation before hydroxylation reactions increased. Despite further hydroxylation, the tricyclic guanidine structure of *m/z = 448* could also be cleaved, which produced *m/z = 418*. In agreement with the literature (He et al., 2014a; Zhang et al., 2015a), this product was only observed for $SO_4^{\bullet-}$-based treatment. However, the following product, which was the result of the loss of the sulfate group (*m/z = 338b*), was observed for both treatments. Hence, for the •OH treatment, *m/z = 418* may have been a transient intermediate product. The product *m/z = 384* could then be produced from *m/z = 464* by removal of the sulfate group.

*3.1.1.3. Attack at the sulfate group.* Fig. 7 shows the degradation pathway focusing on the removal of the sulfate group. The product *m/z = 334b* was either produced directly from CYN by sulfate group removal and dehydrogenation, i.e., the carbonyl group was in the same position as the sulfate group used to be, or via *m/z = 432,* which was monohydroxylated in 1,2-position to the sulfate group, which was then removed. Both forms could then be further hydroxylated at the tricyclic guanidine structure and the hydroxymethyl uracil moiety, forming *m/z = 350b*, *382b*, and *398*. For both treatments, *m/z = 350b* was the most pronounced product for this part of the degradation pathway (Supplementary Fig. S59). As proposed by He et al. (2014b), *m/z = 384* could have been produced from CYN by sulfate group removal and subsequent trihydroxylation via an intermediate product with *m/z = 336* formula $C_{15}H_{21}N_5O_4$. Although we did detect this product, it was not considered a true product peak as the peak area in the samples after treatment was lower than the peak area in the blank and untreated samples and did thus not meet the requirements of the "true product peak criteria". Therefore, we proposed that *m/z = 384* may have also been produced from *m/z = 464* as shown in Fig. 6.

### 3.1.2. CYN degradation mechanisms

Generally, •OH primarily reacts with organic pollutants in three distinctive mechanisms: i) via an electrophilic attack at electron-rich moieties such as aromatic systems, C=C double bonds, and neutral amines, ii) via hydrogen abstraction from C-H groups, and iii) at neutral pH, via an often kinetically unfavored one-electron transfer (Schneider and Bláha, 2020). Reaction mechanisms of $SO_4^{\bullet-}$ have been described to be relatively similar, i.e.: i) via hydrogen abstraction from C-H groups, ii) via an attack at unsaturated bonds, and iii) via electron transfer from carboxylates, amines and aromatic compounds (Schneider and Bláha, 2020). Hence, both treatments were expected to produce similar products, although their quantity may vary. As shown in Supplementary Table S3, from the 116 products that were considered as true product peaks, 17 products were only observed after treatment by $Co^{2+}$/PMS while 16 other products were only observed after treatment by $Fe^{2+}/H_2O_2$. At least for some of these products, this did not necessarily mean that they were not formed during the treatment but rather that they were not formed in high enough quantity to be considered a true product. For instance, the product *m/z = 432* was observed after treatment by $Co^{2+}$/PMS but products that followed in the pathway, e.g. *m/z = 448*, *430* or *334b* were observed after both treatments (see Table 1 and Figs. 2, 6 and 7). In fact, the product *m/z = 432* has previously been reported to be formed by $SO_4^{\bullet-}$- and •OH-based AOPs (He et al., 2014b). Because most degradation products were observed for both treatments, the underlying mechanisms were assumed similar, if not the same. This confirmed what He et al. (2014a) showed in their studies on the degradation of CYN by $SO_4^{\bullet-}$- and •OH-based AOPs. In accordance with other studies, e.g. (He et al., 2014a), the analysis of the products revealed that reactions involved in both degradation processes included hydroxylation, dehydrogenation, decarboxylation, removal of the sulfate group as well as further fragmentation and ring cleavage at the hydroxymethyl uracil moiety and the tricyclic guanidine system (Figs. 2–7). With respect to the quantities of the formed products, the hydroxymethyl uracil ring and the tricyclic guanidine system appeared

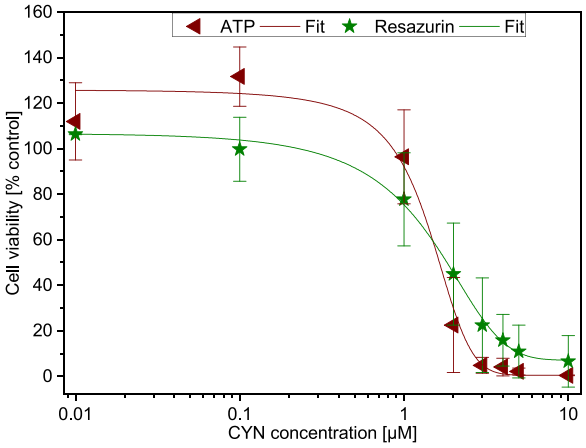


**Fig. 8.** Concentration-response of HepG2 spheroids to untreated CYN in the concentration range of 0.01–10 μM assessed after 96 h of exposure. The symbols show the experimentally derived data while the lines depict the 4-parametric logistic fit into the resazurin ($R^2 = 0.99945$) and ATP ($R^2 = 0.98315$) data. The data is shown as average ± standard deviation from three independent experiments.

to be the primary targets before removal of the sulfate group from the parent toxin (Supplementary Figs. S54–S59). In combination with the results reported by Song et al. (2012), i.e., 84% of •OH produced by radiolysis reacted with the uracil ring, this moiety appeared to be the most crucial functionality within CYN for effective degradation of the toxin by •OH. Similar data is not available for the reaction of CYN with $SO_4^{\bullet-}$. However, due to the high similarity of the degradation

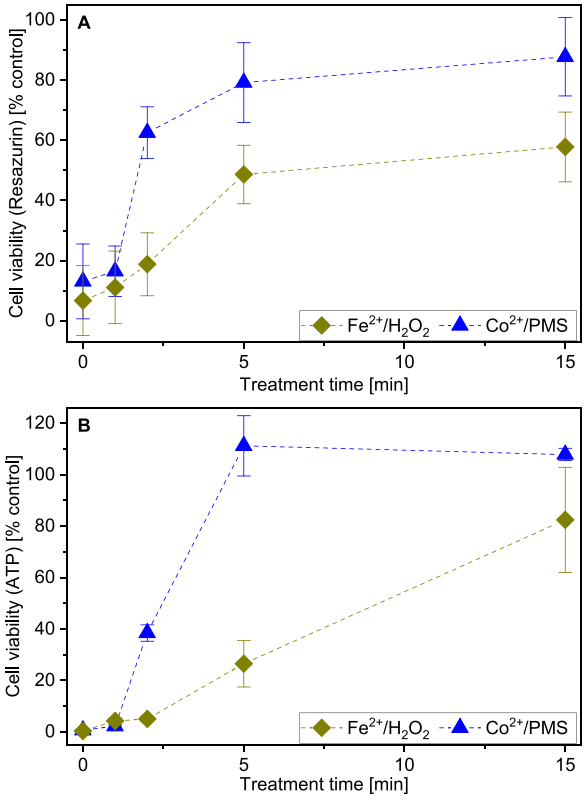


**Fig. 9.** Residual toxicity of CYN treated by $Fe^{2+}/H_2O_2$ and $CO^{2+}$/PMS to HepG2 hepatospheroids after 96 h of exposure assessed by: (A) resazurin and (B) ATP. The data was normalized to the assay blank (no viable cells, 0%) and non-treated spheroids (100%), representing averages ± standard deviation from three independent experiments.

mechanisms, this may also be true for the CYN degradation by $SO_4^{-}\bullet$.

### 3.2. Residual toxicity of treated CYN

The toxicity of the treated CYN was assessed using HepG2 liver cell spheroids. During 96 h of exposure, the size of non-treated spheroids increased from an average of 491 ± 32 μm to 565 ± 54 μm. Untreated CYN at concentrations ≥ 1 μM inhibited spheroid growth and reduced the final spheroid size relative to the control (Supplementary Figs. S60A and S60B). CYN concentrations ≥ 4 μM inhibited spheroid growth practically completely and induced effects comparable to the positive control, 10% (v/v) DMSO. Similar concentration-dependent responses were obtained from the resazurin and ATP assays, with estimated $IC_{50}$ values, i.e., concentrations causing 50% inhibition effect, of 1.8 μM and 1.6 μM, respectively (Fig. 8 and Supplementary Figs. S14C–S14D). At a CYN concentration of 5 μM, both the resazurin conversion and the ATP content were reduced to the levels of the positive control (Supplementary Figs. S60C and S60D) or blank wells, thus providing the maximum assay window to measure the reduction of toxicity in degradation experiments. Therefore, the samples from AOP-treatments were diluted two-fold in the assay to acquire a nominal concentration of 5 μM at $t_0$. The effects of 5 μM of untreated CYN passed through a SPE cartridge were comparable to the same concentration of the toxin added to the spheroids directly, i.e. without SPE passage (Supplementary Figs. S61 and S62). Furthermore, the samples from the blank reaction mixtures without CYN, collected before the initiation of the reaction ($t_0$) and after 15 min of reaction, did not induce effects different from the naïve control (Supplementary Figs. S61 and S62).

After treatment by $Co^{2+}$/PMS and $Fe^{2+}/H_2O_2$, effects of CYN on the spheroid size and viability changed depending on the duration of the AOP treatments, as shown in Fig. 9 and in Supplementary Figs. S61 and S62. Before the AOP treatments, i.e. at $t_0$, CYN reduced the cell viability to below 20% of the control. Contrarily, after 15 min of treatment by $Co^{2+}$/PMS, the cell viability increased to 88 ± 13% for the resazurin assay (Fig. 9A) and 108 ± 2% for the ATP assay (Fig. 9B). This indicated a substantial reduction of the toxicity of the treated CYN solution. Contrarily, after 15 min of treatment by $Fe^{2+}/H_2O_2$, the cell viability increased to 58 ± 12% for the resazurin assay (Fig. 9A) and 82 ± 20% for the ATP assay (Fig. 9B). The effects of both AOP treatments on the cell viability were also reflected by the corresponding reduction of the final spheroid size and the inhibition of their growth as shown in Supplementary Figs. S61A–S61B and S62A–S62B. Although the toxicity of the treated CYN solution was substantially decreased by both AOPs, the •OH-based treatment appeared to be less detoxifying as the $SO_4^{-}\bullet$-based treatment. Indeed, after 15 min of treatment by $Fe^{2+}/H_2O_2$, 1.8 μM of CYN was still left (Fig. 1), which appeared to correspond with the residual toxicity after the Fenton treatment, while for the $Co^{2+}$/PMS treatment only 0.2 μM of CYN was left (Fig. 1). Although the difference in the CYN concentration seemed to be comparatively small, the toxicity steeply decreased between 3.0 and 1.0 μM of CYN as shown in the recorded concentration-response curve for untreated CYN (Fig. 8 and Supplementary Fig. S60). Consequently, a small decrease in the CYN concentration in this range resulted in a substantial increase in the cell viability. Therefore, after 15 min of treatment by both $SO_4^{-}\bullet$ and •OH effectively detoxified the CYN solution.

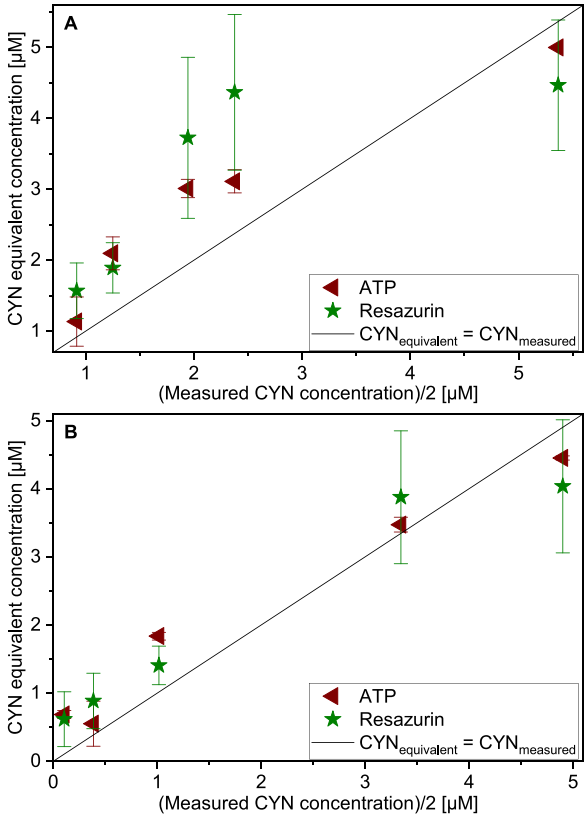


**Fig. 10.** Comparison of CYN equivalent concentrations corresponding to toxicological responses to HepG2 hepatospheroids assessed by ATP and resazurin assays with CYN concentrations measured by LC-DAD after treatment by: (A) $Fe^{2+}/H_2O_2$ and (B) $Co^{2+}$/PMS. The measured CYN concentration was divided by two to adjust for the dilution of the samples before application to the hepatospheroids.

Whether the formed CYN degradation products exhibited toxic effects was further evaluated in more detail by comparing CYN equivalent concentrations, corresponding to the determined toxicological response, with the CYN concentrations measured by LC-DAD. The CYN equivalent concentrations were estimated using a four parametric logistic model that was fitted to the recorded concentration-response curve of untreated CYN (Fig. 8). Fig. 10A and B show the comparison of the CYN equivalent concentrations estimated from the dose-response curve with CYN concentrations determined by LC-DAD for $Co^{2+}$/PMS and $Fe^{2+}/H_2O_2$, respectively. For this comparison, the CYN concentration determined by LC-DAD had to be divided by two to adjust for the dilution of the samples before application of the samples to the hepatospheroids. For both treatments, CYN equivalent concentrations were overestimated except for the highest concentration, which was slightly lower than the concentration determined by LC-DAD (Fig. 10). Due to the S-shape of the concentration-response curves and the relatively narrow concentration range between no-effect concentrations (≤1 μM) and concentrations inducing nearly maximal responses (>4 μM), the models could not accurately determine the CYN equivalent concentrations outside the range of approximately 1–5 μM (Fig. 8). This may have led to the underestimation of the highest CYN equivalent concentrations. As already shown in Fig. 9A, the data derived from the resazurin assay had a higher biological variability that, consequently, resulted in higher variability of the CYN equivalent concentrations determined from the concentration-response curve recorded with the resazurin assay (Fig. 10). The deviation of CYN equivalent concentrations from the instrumentally determined CYN concentrations for the $SO_4^{-}\bullet$-based treatment was relatively small compared with the deviation of CYN equivalent to measured CYN concentrations for the •OH-based treatment (Fig. 10).

An overestimation of the CYN equivalent concentration indicated that the residual CYN concentration determined by LC-DAD could not solely explain the observed toxicological response. Apparently, the initial reduction in CYN toxicity within the first 5 min was slower than the analytically determined decrease in the CYN concentration, especially for the •OH-driven degradation. Consequently, the degradation products formed and abundant in the early phases of the reaction may have been responsible for the toxicity to the HepG2 hepatospheroids. Although the majority of the degradation products formed by reactions with $SO_4^{-}\bullet$ and •OH were qualitatively the same (Figs. 2–7 and Supplementary Table S3), their quantity appeared to differ as shown in the

Supplementary Figs. S54–S59 for the degradation products that were depicted in the proposed degradation pathways. Hence, the difference in the toxicity of the solutions treated by $Co^{2+}$/PMS and $Fe^{2+}/H_2O_2$ may have also been the result of the different quantities of the formed degradation products.

Banker et al. (2001) suggested that the uracil moiety of CYN causes its toxicity as alterations or removal of this specific group substantially reduced its toxicity. However, in their study, only two degradation products were identified and purified before assessing their toxicity (Banker et al., 2001). Furthermore, Cartmell et al. (2017) and Evans et al. (2019) showed that the guanidine moiety and the hydroxyl group in between the uracil and guanidine groups are also crucial for the toxicity. Although the uracil and guanidine moieties were identified as two of the major targets for the degradation of CYN by $SO_4^{\bullet-}$ and •OH (as described in Section 3.1.2), we detected more than 100 potential degradation products. It was not possible to separate the degradation products identified in our study, and the hepatospheroids were exposed to a complex mixture of different degradation products, from which several may have possibly exhibited toxicity. Based on the information from Banker et al. (2001), Cartmell et al. (2017) and Evans et al. (2019), the degradation products that contained the hydroxylmethyl uracil moiety, the guanidine group or a combination of the residues of both groups were most likely the suspects that caused the toxicity to the hepatospheroids.

Contrarily, Yan et al. (2016) observed less deviation of CYN equivalent to measured CYN concentrations when comparing results obtained from the degradation of CYN by ozone and assessing the residual toxicity to 2D-HepG2 cell cultures. Besides the different treatment method, the majority of the degradation products identified by Yan et al. (2016) were the same as in the present study. The hydroxymethyl uracil moiety was suggested to be the most susceptible part for the ozonation of CYN (Yan et al., 2016), and the difference in the accuracy of the estimated CYN equivalent concentrations was most likely related to the toxicological assay. Specifically, Yan et al. (2016) reported $IC_{50}$ values for CYN toxicity in monolayer HepG2 cultures ranging from 8 to 50 μM after 24–48 h of exposure (evaluated by MTS assay), while $IC_{50}$ values observed in our 3D assay after 96 h of exposure were substantially lower (1.8 and 1.6 μM for resazurin and ATP assays, respectively). Human hepatospheroids were previously shown to be more sensitive to CYN in comparison with monolayer cultures (Basu et al., 2018). The higher sensitivity of our approach is likely related to improved hepatocyte-specific functions and consequently, improved sensitivity of HepG2 cells in the 3D cell culture (Gaskell et al., 2016; Hercog et al., 2020; Kim et al., 2019; Štampar et al., 2021). The effective CYN concentrations observed in the present study with HepG2 spheroids were also lower than the 24 h-$IC_{50}$ values reported for differentiated HepaRG cells ranging from 2.6 to 4.1 μM for XTT, NRU or SRB assays (Huguet et al., 2019; Kittler et al., 2016). However, the longer exposure time used in our study (96 h) could be responsible for the relatively lower $IC_{50}$ values, especially for CYN, whose effects in various liver cell types became manifested more progressively with increasing exposure time (López-Alonso et al., 2013; Basu et al., 2018; Raška et al., 2019; Štraser et al., 2013). In this respect, 3D hepatospheroid cultures represent a particularly interesting testing system, in which the cell longevity and liver-like functionality can be maintained for several days or even weeks (Eilenberger et al., 2019; Gaskell et al., 2016), making them suitable for long-term and repeated exposure regimes.

In order to experimentally confirm that some of the CYN degradation products may still be toxic, additional studies would be needed, e.g. testing of only few degradation products at a time (e.g. in an effect-directed analysis approach) or individual products. However, separation of the individual degradation products and production of sufficiently high quantities for the toxicological assessment are technically very difficult. As an alternative approach, the toxicity of synthetic analogs with close structural resemblance to the detected degradation products could be assessed as shown recently (Cartmell et al., 2017; Evans et al., 2019). Regardless of the feasibility of the synthesis of the detected degradation products, both approaches would require much more extensive and laborious experiments, which were beyond the scope of our study.

## 4. Conclusions

The cyanobacterial toxin CYN was effectively degraded by two different radical species, i.e., •OH and $SO_4^{\bullet-}$, produced by Fenton and Fenton-like reactions. The selective radical quenchers EtOH and tBuOH allowed us to infer that the degradation by the Fenton reaction, i.e., $Fe^{2+}/H_2O_2$, was primarily driven by •OH while the Fenton-like reaction, i.e., $Co^{2+}$/PMS, mainly produced $SO_4^{\bullet-}$. Based on more than 100 potential degradation products that were detected, the degradation pathways for the treatment of CYN by •OH and $SO_4^{\bullet-}$ were proposed with the main reaction mechanisms including hydroxylation, dehydrogenation, decarboxylation, removal of the sulfate group as well as further fragmentation and ring cleavage. Although the degradation effectivity of the two radical species appeared to be different, the degradation mechanisms of •OH and $SO_4^{\bullet-}$ were similar, resulting in the same degradation products. The treatment of CYN by Fenton and Fenton-like oxidation led to a reduction in the residual toxicity to HepG2 hepatospheroids. The changes in toxicity coincided with the decrease in the CYN concentration, i.e., detoxification by $SO_4^{\bullet-}$ was more effective than •OH, and the 3D cell model was found highly sensitive for water treatment applications. The comparative analyses further showed that some of the degradation products formed during the CYN treatment might still have exhibited toxicity to the HepG2 cells. In this model study, the initial toxin concentration was high in comparison to actual environmental CYN concentrations, and it can be concluded that under real-life conditions, our initially posed question could be answered positively with "*Yes, degradation of CYN equals its detoxification!*". Based on these promising results, future studies should focus on exploring the applicability and feasibility of •OH and $SO_4^{\bullet-}$, e.g., produced in Fenton and Fenton-like reactions, in drinking water treatment.

## CRediT authorship contribution statement

**Marcel Schneider:** Conceptualization, Methodology, Validation, Formal analysis, Investigation, Resources, Writing – original draft, Visualization, Project administration. **Marina F. Grossi:** Methodology, Validation, Formal analysis, Investigation, Writing – review & editing, Visualization. **Darshak Gadara:** Methodology, Validation, Formal analysis, Investigation, Writing – review & editing, Visualization. **Zdeněk Spáčil:** Validation, Resources, Writing – review & editing, Supervision. **Pavel Babica:** Conceptualization, Methodology, Validation, Formal analysis, Resources, Writing – review & editing, Visualization, Supervision, Project administration, Funding acquisition. **Luděk Bláha:** Conceptualization, Resources, Writing – review & editing, Supervision, Project administration, Funding acquisition.

## Declaration of Competing Interest

The authors declare that they have no known competing financial interests or personal relationships that could have appeared to influence the work reported in this paper.

## Acknowledgement

This research received funding from the European Union's Horizon 2020 research and innovation programme under the Marie Sklodowska-Curie grant agreement No 722493, and was supported from the European Union's Horizon 2020 research and innovation programme under grant agreement No 857560. This publication reflects only the authors' view and the European Commission is not responsible for any use that may be made of the information it contains. Additional funding was

provided by the Czech Science Foundation within the project GA19-19143S. Authors thank to RECETOX RI (No LM2018121) financed by the Ministry of Education, Youth and Sports, and Operational Programme Research, Development and Innovation - project CETOCOEN EXCELLENCE (No CZ.02.1.01/0.0/0.0/17_043/0009632) for supportive background. We would like to thank Dr. Lucie Bláhová for her assistance and advice in the laboratory.

## Appendix A. Supporting information

Supplementary data associated with this article can be found in the online version at doi:10.1016/j.jhazmat.2021.127447.

## References

Adamski, M., Żmudzki, P., Chrapusta, E., Bober, B., Kaminski, A., Zabaglo, K., Latkowska, E., Bialczyk, J., 2016a. Effect of pH and temperature on the stability of cylindrospermopsin. Characterization of decomposition products. Algal Res. 15, 129–134. https://doi.org/10.1016/J.ALGAL.2016.02.020.

Adamski, M., Żmudzki, P., Chrapusta, E., Kaminski, A., Bober, B., Zabaglo, K., Bialczyk, J., 2016b. Characterization of cylindrospermopsin decomposition products formed under irradiation conditions. Algal Res. 18, 1–6. https://doi.org/10.1016/J.ALGAL.2016.05.027.

Anipsitakis, G.P., Dionysiou, D.D., 2004. Radical generation by the interaction of transition metals with common oxidants. Environ. Sci. Technol. 38, 3705–3712. https://doi.org/10.1021/es035121o.

Antoniou, M.G., Shoemaker, J.A., de la Cruz, A.A., Dionysiou, D.D., 2008. LC/MS/MS structure elucidation of reaction intermediates formed during the $TiO_2$ photocatalysis of microcystin-LR. Toxicon 51, 1103–1118. https://doi.org/10.1016/J.TOXICON.2008.01.018.

Banker, R., Carmeli, S., Werman, M., Teltsch, B., Porat, R., Sukenik, A., 2001. Uracil moiety is required for toxicity of the cyanobacterial hepatotoxin cylindrospermopsin. J. Toxicol. Environ. Health Part A 62, 281–288. https://doi.org/10.1080/009841001459432.

Basu, A., Dydowiczová, A., Čtveráčková, L., Jaša, L., Trosko, J.E., Bláha, L., Babica, P., 2018. Assessment of hepatotoxic potential of cyanobacterial toxins using 3D in vitro model of adult human liver stem cells. Environ. Sci. Technol. 52, 10078–10088. https://doi.org/10.1021/acs.est.8b02291.

Basu, A., Dydowiczová, A., Trosko, J.E., Bláha, L., Babica, P., 2020. Ready to go 3D? A semi-automated protocol for microwell spheroid arrays to increase scalability and throughput of 3D cell culture testing. Toxicol. Mech. Methods 30, 590–604. https://doi.org/10.1080/15376516.2020.1800881.

Blahova, L., Sehnal, L., Lepsova-Skacelova, O., Szmucova, V., Babica, P., Hilscherova, K., Teikari, J., Sivonen, K., Blaha, L., 2021. Occurrence of cylindrospermopsin, anatoxin-a and their homologs in the southern Czech Republic – taxonomical, analytical, and molecular approaches. Harmful Algae 108, 102101. https://doi.org/10.1016/j.hal.2021.102101.

Bokare, A.D., Choi, W., 2014. Review of iron-free Fenton-like systems for activating $H_2O_2$ in advanced oxidation processes. J. Hazard. Mater. 275, 121–135. https://doi.org/10.1016/j.jhazmat.2014.04.054.

Brooks, B.W., Lazorchak, J.M., Howard, M.D.A., Johnson, M.-V. v, Morton, S.L., Perkins, D.A.K., Reavie, E.D., Scott, G.I., Smith, S.A., Steevens, J.A., 2016. Are harmful algal blooms becoming the greatest inland water quality threat to public health and aquatic ecosystems? Environ. Toxicol. Chem. 35, 6–13. https://doi.org/10.1002/etc.3220.

Cartmell, C., Evans, D.M., Elwood, J.M.L., Fituri, H.S., Murphy, P.J., Caspari, T., Poniedziałek, B., Rzymski, P., 2017. Synthetic analogues of cyanobacterial alkaloid cylindrospermopsin and their toxicological activity. Toxicol. Vitr. 44, 172–181. https://doi.org/10.1016/j.tiv.2017.07.007.

Chen, L., Zhao, C., Dionysiou, D.D., O'Shea, K.E., 2015. $TiO_2$ photocatalytic degradation and detoxification of cylindrospermopsin. J. Photochem. Photobiol. A: Chem. 307–308, 115–122. https://doi.org/10.1016/J.JPHOTOCHEM.2015.03.013.

Costa, E.C., Moreira, A.F., de Melo-Diogo, D., Gaspar, V.M., Carvalho, M.P., Correia, I.J., 2016. 3D tumor spheroids: an overview on the tools and techniques used for their analysis. Biotechnol. Adv. 34, 1427–1441. https://doi.org/10.1016/j.biotechadv.2016.11.002.

Eilenberger, C., Rothbauer, M., Ehmoser, E.-K., Ertl, P., Küpcü, S., 2019. Effect of spheroidal age on sorafenib diffusivity and toxicity in a 3D HepG2 spheroid model. Sci. Rep. 9, 4863. https://doi.org/10.1038/s41598-019-41273-3.

Evans, D.M., Hughes, J., Jones, L.F., Murphy, P.J., Falfushynska, H., Horyn, O., Sokolova, I.M., Christensen, J., Coles, S.J., Rzymski, P., 2019. Elucidating cylindrospermopsin toxicity via synthetic analogues: an in vitro approach. Chemosphere 234, 139–147. https://doi.org/10.1016/j.chemosphere.2019.06.021.

Fotiou, T., Triantis, T., Kaloudis, T., Hiskia, A., 2015. Photocatalytic degradation of cylindrospermopsin under UV-A, solar and visible light using $TiO_2$. Mineralization and intermediate products. Chemosphere 119, S89–S94. https://doi.org/10.1016/J.CHEMOSPHERE.2014.04.045.

Gaskell, H., Sharma, P., Colley, H.E., Murdoch, C., Williams, D.P., Webb, S.D., 2016. Characterization of a functional C3A liver spheroid model. Toxicol. Res. 5, 1053–1065. https://doi.org/10.1039/c6tx00101g.

Ghanbari, F., Moradi, M., 2017. Application of peroxymonosulfate and its activation methods for degradation of environmental organic pollutants: review. Chem. Eng. J. 310, 41–62. https://doi.org/10.1016/j.cej.2016.10.064.

He, X., de la Cruz, A.A., O'Shea, K.E., Dionysiou, D.D., 2014a. Kinetics and mechanisms of cylindrospermopsin destruction by sulfate radical-based advanced oxidation processes. Water Res. 63, 168–178. https://doi.org/10.1016/J.WATRES.2014.06.004.

He, X., Zhang, G., de la Cruz, A.A., O'Shea, K.E., Dionysiou, D.D., 2014b. Degradation mechanism of cyanobacterial toxin cylindrospermopsin by hydroxyl radicals in homogeneous UV/$H_2O_2$ process. Environ. Sci. Technol. 48, 4495–4504. https://doi.org/10.1021/es403732s.

Hercog, K., Štampar, M., Štern, A., Filipič, M., Žegura, B., 2020. Application of advanced HepG2 3D cell model for studying genotoxic activity of cyanobacterial toxin cylindrospermopsin. Environ. Pollut. 265, 114965 https://doi.org/10.1016/j.envpol.2020.114965.

Huguet, A., Lanceleur, R., Quenault, H., le Hégarat, L., Fessard, V., 2019. Identification of key pathways involved in the toxic response of the cyanobacterial toxin cylindrospermopsin in human hepatic HepaRG cells. Toxicol. Vitr. 58, 69–77. https://doi.org/10.1016/j.tiv.2019.03.023.

Ike, I.A., Linden, K.G., Orbell, J.D., Duke, M., 2018. Critical review of the science and sustainability of persulphate advanced oxidation processes. Chem. Eng. J. 338, 651–669. https://doi.org/10.1016/j.cej.2018.01.034.

Ji, X.-X., Wang, H.-F., Hu, P.-J., 2019. First principles study of Fenton reaction catalyzed by FeOCl: reaction mechanism and location of active site. Rare Met. 38, 783–792. https://doi.org/10.1007/s12598-018-1140-9.

Kim, B.-Y., Kim, M., Jeong, J.S., Jee, S.-H., Park, I.-H., Lee, B.-C., Chung, S.-K., Lim, K.-M., Lee, Y.-S., 2019. Comprehensive analysis of transcriptomic changes induced by low and high doses of bisphenol A in HepG2 spheroids in vitro and rat liver in vivo. Environ. Res. 173, 124–134. https://doi.org/10.1016/j.envres.2019.03.035.

Kittler, K., Hurtaud-Pessel, D., Maul, R., Kolrep, F., Fessard, V., 2016. In vitro metabolism of the cyanotoxin cylindrospermopsin in HepaRG cells and liver tissue fractions. Toxicon 110, 47–50. https://doi.org/10.1016/j.toxicon.2015.11.007.

León, C., Boix, C., Beltrán, E., Peñuela, G., López, F., Sancho, J. v, Hernández, F., 2019. Study of cyanotoxin degradation and evaluation of their transformation products in surface waters by LC-QTOF MS. Chemosphere 229, 538–548. https://doi.org/10.1016/j.chemosphere.2019.04.219.

Liu, J., Hernández, S.E., Swift, S., Singhal, N., 2018. Estrogenic activity of cylindrospermopsin and anatoxin-a and their oxidative products by $Fe^{III}$-B*/$H_2O_2$. Water Res. 132, 309–319. https://doi.org/10.1016/J.WATRES.2018.01.018.

López-Alonso, H., Rubiolo, J.A., Vega, F., Vieytes, M.R., Botana, L.M., 2013. Protein synthesis inhibition and oxidative stress induced by cylindrospermopsin elicit apoptosis in primary rat hepatocytes. Chem. Res. Toxicol. 26, 203–212. https://doi.org/10.1021/tx3003438.

Martínez-Ruiz, E.B., Cooper, M., Al-Zeer, M.A., Kurreck, J., Adrian, L., Szewzyk, U., 2020. Manganese-oxidizing bacteria form multiple cylindrospermopsin transformation products with reduced human liver cell toxicity. Sci. Total Environ. 729, 138924 https://doi.org/10.1016/j.scitotenv.2020.138924.

Merel, S., Clément, M., Mourot, A., Fessard, V., Thomas, O., 2010. Characterization of cylindrospermopsin chlorination. Sci. Total Environ. 408, 3433–3442. https://doi.org/10.1016/j.scitotenv.2010.04.033.

Ministry of Health, 2017. Guidelines for Drinking-water Quality Management for New Zealand, third ed. Ministry of Health, Wellington.

Neale, P.A., O'Brien, J.W., Glauch, L., König, M., Krauss, M., Mueller, J.F., Tscharke, B., Escher, B.I., 2020. Wastewater treatment efficacy evaluated with in vitro bioassays. Water Res. X 9, 100072. https://doi.org/10.1016/j.wroa.2020.100072.

Raška, J., Čtveráčková, L., Dydowiczová, A., Sovadinová, I., Bláha, L., Babica, P., 2019. Cylindrospermopsin induces cellular stress and activation of ERK1/2 and p38 MAPK pathways in adult human liver stem cells. Chemosphere 227, 43–52. https://doi.org/10.1016/j.chemosphere.2019.03.131.

Scarlett, K.R., Kim, S., Lovin, L.M., Chatterjee, S., Scott, J.T., Brooks, B.W., 2020. Global scanning of cylindrospermopsin: critical review and analysis of aquatic occurrence, bioaccumulation, toxicity and health hazards. Sci. Total Environ. 738, 139807 https://doi.org/10.1016/j.scitotenv.2020.139807.

Schneider, M., Bláha, L., 2020. Advanced oxidation processes for the removal of cyanobacterial toxins from drinking water. Environ. Sci. Eur. 32, 94. https://doi.org/10.1186/s12302-020-00371-0.

Schneider, M., Rataj, R., Kolb, J.F., Bláha, L., 2020. Cylindrospermopsin is effectively degraded in water by pulsed corona-like and dielectric barrier discharges. Environ. Pollut. 266, 115423 https://doi.org/10.1016/j.envpol.2020.115423.

Song, W., Yan, S., Cooper, W.J., Dionysiou, D.D., O'Shea, K.E., 2012. Hydroxyl radical oxidation of cylindrospermopsin (Cyanobacterial Toxin) and its role in the photochemical transformation. Environ. Sci. Technol. 46, 12608–12615. https://doi.org/10.1021/es302458h.

Štampar, M., Sedighi Frandsen, H., Rogowska-Wrzesinska, A., Wrzesinski, K., Filipič, M., Žegura, B., 2021. Hepatocellular carcinoma (HepG2/C3A) cell-based 3D model for genotoxicity testing of chemicals. Sci. Total Environ. 755, 143255 https://doi.org/10.1016/j.scitotenv.2020.143255.

Štraser, A., Filipič, M., Novak, M., Žegura, B., 2013. Double strand breaks and cell-cycle arrest induced by the cyanobacterial toxin cylindrospermopsin in HepG2 Cells. Mar. Drugs 11, 3077–3090. https://doi.org/10.3390/md11083077.

Triantis, T.M., Kaloudis, T., Hiskia, A., 2016. Solid-phase extraction of cylindrospermopsin from filtered and drinking water. In: Meriluoto, J., Spoof, L., Codd, G.A. (Eds.), Handbook of Cyanobacterial Monitoring and Cyanotoxin Analysis. Wiley Online Books, pp. 396–398. https://doi.org/10.1002/9781119068761 ch47.

Verma, S., Nakamura, S., Sillanpää, M., 2016. Application of UV-C LED activated PMS for the degradation of anatoxin-a. Chem. Eng. J. 284, 122–129. https://doi.org/10.1016/J.CEJ.2015.08.095.

Wang, S., Ma, W., Fang, Y., Jia, M., Huang, Y., 2014. Bismuth oxybromide promoted detoxification of cylindrospermopsin under UV and visible light illumination. Appl. Catal. B: Environ. 150–151, 380–388. https://doi.org/10.1016/J.APCATB.2013.12.016.

Wang, S., Chen, Y., Jiao, Y., Li, Z., 2019. Detoxification of cylindrospermopsin by pyrite in water. Catalysts 9, 699. https://doi.org/10.3390/catal9090699.

World Health Organization, 2020. Cyanobacterial toxins: cylindrospermopsins. World Health Organization, Geneva PP - Geneva.

Wu, C.-C., Huang, W.-J., Ji, B.-H., 2015. Degradation of cyanotoxin cylindrospermopsin by $TiO_2$-assisted ozonation in water. J. Environ. Sci. Health Part A Toxic/Hazard. Subst. Environ. Eng. 50, 1116–1126. https://doi.org/10.1080/10934529.2015.1047664.

Yan, S., Jia, A., Merel, S., Snyder, S.A., O'Shea, K.E., Dionysiou, D.D., Song, W., 2016. Ozonation of cylindrospermopsin (cyanotoxin): degradation mechanisms and cytotoxicity assessments. Environ. Sci. Technol. 50, 1437–1446. https://doi.org/10.1021/acs.est.5b04540.

Zeng, H., Zhao, X., Zhao, F., Park, Y., Repo, E., Thangaraj, S.K., Jänis, J., Sillanpää, M., 2020. Oxidation of 2,4-dichlorophenol in saline water by unactivated peroxymonosulfate: mechanism, kinetics and implication for in situ chemical oxidation. Sci. Total Environ. 728, 138826 https://doi.org/10.1016/j.scitotenv.2020.138826.

Zhang, G., He, X., Nadagouda E., M.N., O'Shea, K., Dionysiou, D.D., 2015a. The effect of basic pH and carbonate ion on the mechanism of photocatalytic destruction of cylindrospermopsin. Water Res. 73, 353–361. https://doi.org/10.1016/J.WATRES.2015.01.011.

Zhang, G., Wurtzler, E.M., He, X., Nadagouda, M.N., O'Shea, K., El-Sheikh, S.M., Ismail, A.A., Wendell, D., Dionysiou, D.D., 2015b. Identification of $TiO_2$ photocatalytic destruction byproducts and reaction pathway of cylindrospermopsin. Appl. Catal. B: Environ. 163, 591–598. https://doi.org/10.1016/J.APCATB.2014.08.034.

Zhang, X., Jiang, T., Chen, D., Wang, Q., Zhang, L.W., 2020. Three-dimensional liver models: state of the art and their application for hepatotoxicity evaluation. Crit. Rev. Toxicol. 50, 279–309. https://doi.org/10.1080/10408444.2020.1756219.